

AVO analysis and complex attributes for a Glauconitic gas sandbar

Hai-man Chung and Don C. Lawton

ABSTRACT

A Glauconitic gas-bearing sandbar from Southern Alberta was studied in terms of its AVO behavior and complex attributes. The seismic data reveals an interesting anomaly in the full-offset stack. In particular, the anomaly appears clearly in the near-offset stack (0-1050 meters) but is poorly outlined in the mid-offset stack (1050-2100 meters). Subsequent AVO modelling indicates that in the subject area under study, for the Glauconitic Formation, thin-bed tuning effects overwhelm any AVO effects due to lateral changes of lithology for offsets up to 3000 meters. The differences of the anomaly as it appears in the near-offset and mid-offset stacks can be largely attributed to a lower frequency content in the mid-offset stack.

The complex attributes plots show corresponding differences of the anomaly in the various offsets attributes plots. In particular, the instantaneous frequency plot for the near-offset stack reveals the anomaly distinctly, but it is virtually absent on the corresponding plot for the mid-offset stack. It is evident that complex attributes plots are very sensitive to the frequency content of the seismic data.

PROJECT OBJECTIVE

In recent years, the subject of amplitude variation with offset(AVO) analysis has attracted much attention among exploration geophysicists. This is mainly due to the potential capability of AVO analysis of seismic data to delineate clastic gas reservoirs, as discussed by Ostrander (1984). However, in addition to the lateral change of the Poisson's ratio due to the presence of gas sands, many other physical factors, such as thin-bed tuning, also contribute to AVO effects. Therefore, the method should be studied further to enhance our understanding of its usefulness and pitfalls.

The applications of complex attributes to seismic signal analysis were first discussed by Taner (1977,1979). In the ensuing years up to the present time, there have been only three other papers published in Geophysics on the same subject, of which the paper by Robertson and Nogami (1984) is the only one that deals with thin-bed effects. No doubt, more papers need to be published on the successes and failures of the usage of complex attributes in exploration in order to promote further understanding and development of the subject.

One of the objectives of the Crewes project is to study the AVO analysis and complex attributes of both P-wave and S-wave seismic data. In particular, their ability to delineate thin beds will be investigated. This paper is the first step in the study, and involves only P-wave data. It is a case study of a gas-bearing Glauconitic sandbar in Southern Alberta. The reader is assumed to be familiar with the theories of both AVO analysis and complex attributes, as they will not be discussed here. For review of these subjects, the papers by Ostrander (1984), Taner (1977,1979), and Robertson and Nogami (1984) are excellent references.

INTRODUCTION

In early 1986, Summit Resources and Alberta Energy Company decided to template a Glauconitic gas well in Southern Alberta with a 3 km long seismic line. The purpose was to investigate the seismic signature of the gas-bearing sandbar. Since the well does not have a sonic log, no forward seismic modelling could be performed. Geophysically, shooting a seismic line over the well is perhaps the most effective way to study the sandbar in the absence of a corresponding sonic log.

A 21-fold seismic line was subsequently shot over the well in the latter part of January, 1986. The seismic data revealed a significant anomaly over the well location. There was drupe over the sandbar, phase reversal due to saturated gas sands, and an apparent Mississippian low structure below the gas sands.

The objective of the case study is to investigate the channel sand anomaly in terms of AVO effects and complex attributes. In particular, complex attributes as a function of source-receiver offsets will be examined. Because of confidentiality, all seismic shotpoint location numbers will be omitted, and the wells will be referred to symbolically without revealing their true locations.

GEOLOGICAL BACKGROUND

In the subject area under study, the Upper Mannville Glauconitic Formation is represented by two lithofacies, (a) regional sequence, and (b) channel features which are shale and sand-filled. The regional sequence consists of a shoaling upward cycle from the Ostracod limestones and Bantry shales. The shoaling sequence carries through to delta plain carbonaceous shales and coals. Delta front sands and localized shoreface sands within the regional sequence can form thin reservoirs if trapping by channel truncation and/or sufficient structural reversal occurs. The entire sequence from Ostracod to delta plain is rarely more than 40 meters in thickness.

Following the deposition of the regional sequence, a series of major channels down-cut through it and generally, but not always, also through the underlying Ostracod and Bantry Formations. Within the channels, large discrete bars of varying thicknesses were deposited which can completely fill the channel with a single clean, medium to coarse grain quartzose sandbar. The sandbars can be up to 40 meters thick with an areal extent of up to a section, though half a section is more common.

The subject well penetrated a 40-meter channel section and complete truncation and removal of the Ostracod/Bantry section has occurred. The channel fill consists of a thick 21-meter basal sand over which lies 18 meters of silty/sandy shale and a 1-meter layer of carbonaceous shale which caps the entire channel fill sequence. Logs indicate that the sandbar has an average porosity of 23%. Production testing and log analysis indicate that eight meters of gas pay are present over a 13-meter water leg within the channel sand. Reserves are estimated at about five billion cubic feet.

Figure 1 shows the interpreted channel position in the area, the locations of the subject well (E) and neighboring wells, and the location of the template seismic line. Figure 2 is a structural cross-section through the subject well (E) and some of the neighboring wells. It clearly illustrates the channeling event through the subject well, with the porous sands highlighted in yellow and the gas-producing zone in red.

ACQUISITION AND PROCESSING

The seismic line was acquired with P vibrators as the energy source, and was recorded as sign-bit signals. The following chart summarizes the acquisition parameters:

spread:	1600-25-0-25-1600 meters (0-25-3200 meters for first roll-in and last roll-out shots)
source interval:	75 meters
receiver interval:	25 meters
source:	Vibroseis, 4 Mertz vibrators over 32 meters, 12 sweep at 14 seconds, 13-55 Hz, 16-59 Hz, 18-63 Hz, 22-67 Hz, 26- 71 Hz, 28-75 Hz, upsweep and downsweep
receivers:	Mark L-28, 10 Hz, 9 at 2.7 meters
instruments:	Geocor IV, 128 trace
fold coverage :	21
sample rate:	2 ms
field filters:	out-out, notch out

The seismic line was processed by Seis-pro Consultants Ltd. The various stack sections indicate that the data have good signal-to-noise ratio. Because we are interested in analyzing amplitude variation with offset, every effort was made to preserve true relative amplitudes. This includes application of gain to compensate for spherical divergence without any trace equalization before deconvolution. For the deconvolution, a surface-consistent shot deconvolution was applied. In other words, one single deconvolution operator, which was obtained as an average over all traces belonging to the same shot, was applied to those traces. This contrasts with the normal procedure of obtaining one deconvolution operator for each trace and applying it to that trace alone. The surface-consistent deconvolution is an attempt to preserve the amplitude characteristics for each wavelet corresponding to each shot. After stacking, long-window rms scaling was applied to each trace to ensure that their rms amplitudes do not significantly differ from each other. The following chart summarizes the processing steps:

1. demultiplex
2. gain - spherical divergence only, no trace equalization
3. geophone phase compensation

4. surface-consistent shot deconvolution
5. elevation and weathering corrections
6. NMO correction - first pass
7. surface-consistent statics
8. NMO correction - second pass
9. gather
10. trim statics
11. stack - 21 fold
12. filter - bandpass, 10/15 - 75/85 Hz
13. scaling - multigate window, 50 to 350 ms, 350 to 1600 ms

Figure 3 shows a normal polarity display of the final stack. The gas-bearing sandbar is represented by the boxed anomaly. Here one can observe drape over the gas sands, phase reversal probably due to their low velocity, and a Mississippian low. Moreover, the amplitudes of the peaks along the drape above the sandbar decrease over the sandbar, while the reversal also shows clear amplitude variations. In the following two sections, we will analyze this anomaly in terms of amplitude-versus-offset effects and complex attributes.

AMPLITUDE VARIATION WITH OFFSET ANALYSIS (AVO)

To investigate the AVO effects of the gas-bearing sandbar, three partial stacks were generated. The first one, the near-offset stack, covers the distance of 0 to 1050 meters, the second one, the mid-offset stack, 1050 to 2100 meters, and the third one, the far-offset stack, 2100 to 3175 meters. However, to cancel noise due to surface waves, the far-offset stack was muted to below the zone of interest, which is about 1000 ms. Hence, we will not discuss the far-offset stack, and effectively, we have offsets only up to 2100 meters.

Figures 4, 5, and 6 show the seismic anomaly for full-offset stack, near-offset stack, and mid-offset stack respectively. The anomaly appears to be significantly different on the near-offset stack than on the mid-offset stack. The full-offset stack is the average of the other two. The anomaly in the near-offset stack has a distinct phase reversal signature. The drape on top of the sandbar is also very evident in this stack. However, the apparent delay in the Mississippian event that is clear on both the full-offset and mid-offset stacks does not appear in the near-offset stack. On the other hand, in the mid-offset stack, the anomaly appears as a very broad and lower-frequency wavelet without showing any overlying drape nor clear reversal character.

To attempt to explain the differences in the two stacks, the first step is to investigate the possibility of the differences as a result of changes in Poisson's ratio. Since low-velocity saturated gas-sands have relatively low Poisson's ratios, they often show up as amplitude anomalies when the corresponding seismic data are displayed in some offset-dependent format such as CDP gather panels (Ostrander, 1984). Figure 7 shows the Ostrander gather (Ostrander, 1984) for four CDP locations along the seismic template line. To obtain the gather, six CDP panels across each location are summed with a three-offsets range for each output trace. In other words, each trace on the Ostrander gather in figure 7 is the sum of eighteen traces. This effectively smears the reflections over six CDP locations, that is over 62.5 meters and for an offset range of 75 meters. However, the signal-to-noise ratio is also enhanced by a factor of four. Note that there is no trace balancing applied to the data. CDP locations A and B are regional Glauconitic locations, and CDP location C is the channel edge location. All three locations show similar

characters at the Glauconite to Mississippian interval, with relative strong peaks for the Glauconitic reflections. However, CDP location D, which is where the gas-bearing sandbar is situated, shows remarkably different results. The Glauconitic reflections have very low amplitudes for the first three near-offset traces, then appear as low-amplitude doublets for the mid-offset traces, and finally turn into high-amplitude single peaks with some evidence of NMO stretch. In fact, it appears that the Glauconitic reflections reverse polarity over the mid-offset traces.

To further understand these seismic character changes, AVO analyses were performed on three wells, using the Hampson-Russell AVO modelling package. In this package, ray tracing is performed, and reflection coefficients are calculated by solving the Zoeppritz equations for specified offsets up to the critical distance. One inputs the sonic log and density log, and the package will assign an initial value of 0.25 for the Poisson's ratio for all layers, which can be modified as desired. A peak frequency of 31 Hz and a maximum offset of 3000 meters are used in all the AVO synthetics. For each well chosen for AVO analysis, two synthetics will be generated. The first one will be a NMO corrected synthetic, where ray-tracing is first performed, and then NMO correction is applied. The second one will be a plane-wave solution synthetic, where every trace is a zero-offset trace, although the reflection coefficients are still offset-dependent. This synthetic will allow us to investigate AVO effects as predicted by Zoeppritz equation without the interference of thin-bed tuning and NMO stretch effects.

The chosen wells are (B) (figure 1), a Glauconitic channel gas well; (C), a Glauconitic channel shale well (also a gas well from another formation); and (F), a Glauconitic regional well. The well (B) has lithologies similar to that of the subject well (E); since (E) does not have a sonic log, the thicknesses of the two lithological units in the Glauconitic Formation in (B) are modified to reflect the corresponding thicknesses in (E). Figures 8 and 9 show the results of the AVO modelling on this modified sonic log for two values of the Poisson's ratio for the gas-bearing sands. In figures 8a, 8b, and 8c, the Poisson's ratio is 0.1. In figures 9a, 9b, and 9c, it is 0.25. In both cases, the P-wave reflection coefficients are negative, reflecting the low-velocity porous sands. However, in figure 8a, where the Poisson's ratio is 0.1, the P-wave reflection coefficients do not change appreciably for offsets less than 2000 meters. The corresponding NMO corrected synthetic (figure 8b) shows some noticeable amplitude changes at an offset of 1800 meters or larger, while NMO-stretch effects are observable at about 2400 meters and larger offsets. On the other hand, the plane-wave solution synthetic (figure 8c) reveals hardly any amplitude changes. When the Poisson's ratio is changed to 0.25, reflecting the situation of non-gaseous sands, the P-wave reflection coefficients (figure 9a) are still negative but they show more variations with offset than that of the gaseous sands. However, the situation with the synthetics is the same as before. The NMO-corrected synthetic (figure 9b) starts to show some significant amplitude changes at an offset of 1800 meters, with strong NMO stretch effects at 2400 meters and larger offsets. The corresponding plane-wave solution synthetic reveals no significant amplitude changes with offset.

Figures 10a, 10b, and 10c are the models for (C), which is a channel silty-shale well. The P-wave reflection coefficients (figure 10a) for the Glauconitic Formation are positive and start to change significantly only for offsets greater than 2400 meters. Both the NMO corrected synthetic (figure 10b) and the plane-wave solution synthetic (figure 10c) reveal insignificant amplitude changes as a function of offset.

Figures 11a, 11b, and 11c are the models for (F), which is a Glauconitic regional well. The P-wave reflection coefficients (figure 11a) show similarity to those of (C). The two synthetics (figures 11b and 11c) show similar results to those of figures 8b and 8c. In other words, the NMO corrected synthetics show some significant amplitude changes at 1800 meters or larger offsets, but the plane-wave solution synthetic shows negligible amplitude changes with offset.

The three sets of models seem to imply that any observable AVO effects for offsets of 2500 meters or less are probably thin-bed tuning effects. The magnitude of the offset-

dependent reflection coefficients calculated from Zoeppritz equations do not show any significant P-wave changes for offsets below 2400 meters in all cases except in the case of figure 9a. Nevertheless, in all four cases, once thin-bed tuning effects are eliminated as in the plane-wave solution synthetics, there are hardly any detectable amplitude variations with offset.

Since the near-offset stack appears to have a higher frequency content than the mid-offset stack, the near-offset stack was then filtered four times, each time with a different filter. The results are shown in figures 12 to 15. In figure 12, where the filter is 8/16-35/40 Hz, the phase reversal disappears completely, while the drape is barely observable but with clear amplitude changes. Obviously, the frequency content is too low to reveal the anomaly. In figure 13, the filter is 8/16-40/45 Hz. The anomaly on this stack shares some interesting similarity to that in the mid-offset stack. Both stacks show broad wavelets for the anomaly with similar looking bandwidths. This seems to imply that the differences in the anomaly as it appears in the near-offset and mid-offset stacks can be partly attributed to a lower frequency content in the mid-offset stack. Figures 14 and 15 have filters 8/16-45/50 and 8/16-50/55 respectively. They indicate that with frequencies higher than 45 Hz present in the data, the near-offset stack starts to develop a relatively distinct character for the anomaly.

COMPLEX ATTRIBUTES

Another objective of this case history is to examine the complex attributes of the anomaly. In particular, we want to examine the complex attributes of the anomaly for various offsets. To make the discussion clearer, we shall discuss the attributes separately. The attributes are calculated by the GMA Grits package.

(a) Instantaneous amplitude

The instantaneous amplitude is sometimes called the amplitude envelope or the reflection strength. It is simply the amplitude of the complex trace, and is phase-independent (Taner, 1979). Figure 16, 17, and 18 are the amplitude envelopes for the full-offset stack, the near-offset stack, and the mid-offset stack respectively. The channel is clearly visible in both the full-offset and near-offset amplitude envelopes, but is virtually unobservable in the mid-offset stack amplitude envelope. Since the mid-offset stack has a lower frequency content than the other two stacks, its amplitude envelope also appears to have lower frequency content than the other two envelopes. The lower frequency content seems to cause the disappearance of the channel signature in the mid-offset amplitude envelope.

(b) Instantaneous phase

Figures 19, 20, and 21 are the instantaneous phase plots for the full-offset stack, the near-offset stack, and the mid-offset stack respectively. As pointed out by both Tanner (1979) and Robertson et al. (1984), instantaneous phase is a very effective tool for delineating discontinuities, faults, pinchouts, angularities and events with different dip attitudes. This is mainly due to the fact that the instantaneous phase is independent of amplitude. Hence, discontinuities that are difficult to observe on conventional seismic data due to low amplitudes will show up more clearly on phase displays. Therefore, the subject

channel anomaly should be nicely outlined on the instantaneous phase plots for the full-offset stack and the near-offset stack. In particular, on the one for the near-offset stack (figure 20), along the time of 0.98 to 1.0 second, discontinuities that are likely channel edge effects can be seen at trace 22 and between traces 71 and 85. However, the channel anomaly is not detectable in the mid-offset instantaneous phase plot (figure 21), nor are there any channel edge effects. It also appears to have lower frequency content than the other two phase plots.

Incidentally, there is an event detected in the mid-offset stack phase plot that appears to be very different in the near-offset phase plot. The event at about 1.020 seconds between traces 53 to 71 on the mid-offset phase plot appears to have been truncated at both ends, and causes some drape on top. The corresponding event in the near-offset phase plot, however, is rather continuous. This event is probably the Mississippian reflections. Given the differences in the Mississippian reflection characters on the two stacks, it is not surprising that the corresponding instantaneous phase plots also exhibit differences. Since the Glauconitic reflection is typically only about 30 ms above the Mississippian reflection, it would be very useful to explain the AVO behavior of the latter.

(c) Instantaneous frequency

Figures 22, 23, and 24 are the instantaneous frequency plots for the full-offset stack, the near-offset stack, and the mid-offset stack respectively. Since the instantaneous frequency is the time derivative of the instantaneous phase, it is also amplitude-independent. For this attribute, only the near-offset instantaneous frequency plot shows the anomaly unequivocally with a dipping event between traces 23 and 40 at about 0.98 seconds. It is virtually absent on the other two frequency plots. This seems to imply that, among the three attributes, the instantaneous frequency is the best tool to outline the channel anomaly. This is probably true whenever a thin bed is involved. Robertson et al. (1984) reported that as a bed thins to a quarter period of the dominant wavelength, there is an anomalous increase in instantaneous frequency, which remains high as the bed continues to thin. This agrees with Widess's (1973) conclusion that when the bed thins to below tuning thickness, the wavelet shape will assume the shape of its derivative and remain constant until the thickness approaches zero, while its amplitude will also decrease to zero. As mentioned earlier, our subject gas-bearing sandbar is only 8 meters thick, and is below tuning thickness, assuming a peak frequency of 40 Hz. and a Glauconitic sand velocity of 3700 meters/second, which gives a tuning thickness of 23 meters. Hence, it should show up in the instantaneous frequency plot. However, it is interesting to note that the gas-sand anomaly appears only in the near-offset stack instantaneous frequency plot, but not in the other two frequency plots. Obviously, the instantaneous frequency attribute is very sensitive to the frequency content of the data. Note that the "low-frequency shadow" reported by Taner (1979) is not observable on any of the frequency plots.

DISCUSSION

The Glauconitic sandbar in the subject well (E) exhibited an interesting anomaly on conventional seismic data. Although the channel section is 40 meters thick, only 8 meters of it are gas-bearing. Assuming a peak frequency of 40 Hz and a sand velocity of 3700 meters/second, the tuning thickness would be about 23 meters. Hence, the gas-bearing zone is well below tuning thickness. This, in turn, means that to fully understand the amplitude behavior of the anomaly, one should also investigate the effect of tuning on

amplitude changes at non-normal incidence. In particular, in Alberta, the AVO effects of many thin hydrocarbon-bearing reservoirs are often negated by their tuning effects. Therefore, for thin beds below tuning thicknesses, no AVO analyses are complete without corresponding thin-bed tuning analyses. Nevertheless, the AVO analyses performed on the three wells are still informative in a qualitative manner. First of all, the analyses imply that for the Glauconitic Formation in Southern Alberta, AVO effects due to a lateral change of lithology can be observed, if at all, only for offsets well over 2500 meters. For our seismic template line, the largest offset is 2100 meters, with any larger offsets being muted out for the Glauconitic reflection in order to cut down noise due to surface waves. Hence, one could not observe any conclusive evidence for AVO effects as a result of a lateral change in the Poisson's ratio of the gas-bearing sand between the near-offset stack and the mid-offset stack, notwithstanding the presence of other character differences. This also means that in any Southern Alberta area where the surface-waves noise requires a relatively severe mute so that any offsets above 2500 meters have to be muted to below the Glauconitic reflection, the AVO method may not be an appropriate tool. Even for areas where the near-surface condition is excellent resulting in a very shallow mute, offsets much larger than 2500 meters are probably required before any AVO effects could be clearly detected, if one takes into consideration other noise problems present in seismic data.

Secondly, the AVO analyses clearly indicate that, in the subject area under study, as far as the Glauconitic Formation is concerned, thin-bed tuning effects dominate any AVO effects due to lateral changes in the Poisson's Ratio. Furthermore, NMO-stretch effects for long offset traces are evident on all the synthetics. This also makes any AVO effects due to lateral changes of lithology more difficult to observe on large offset traces, since it lowers the frequency of those traces. The differences of the anomaly between the near-offset stack and the mid-offset stack are probably largely due to lower frequency content in the mid-offset stack. On the other hand, the differences in the Mississippian reflection between the two stacks simply cannot be explained by a difference in frequency alone, nor can it be explained by AVO effects, since apparent structural differences exist. Is it possible that different offsets would reveal structural elements preferentially? It would be interesting to investigate this possibility.

The complex attributes for the various offsets indicate that the channel can be recognized clearly on data with frequency of 45 Hz or higher present. The instantaneous phase outlines the lateral discontinuities at the channel edge remarkably well for the near-offset stack. In particular, the instantaneous frequency is very useful in delineating beds that are thinner than tuning thickness. Furthermore, the differences between the instantaneous phase and frequency plots for the near-offset and mid-offset stacks suggest that the attributes are very sensitive to the frequency content of the seismic data. Thus, it would be a very useful exercise to study how the frequency content of the attributes relate to the frequency content of the corresponding seismic data.

Another potential use of the instantaneous phase and frequency is the possibility of delineating a wedge-shaped thin bed. Since the wavelet shape undergoes a definite pattern change as the bed thins from above tuning thickness to zero thickness, the instantaneous phase and frequency plots will outline the change very clearly, since they are independent of the amplitude.

CONCLUSION

This case study does not reveal any significant AVO effects due to a lateral decrease in the Poisson's ratio of the Glauconitic gas-bearing sands for the modified well (B) for offsets up to 3000 meters. However, the differences in the characters of the anomaly between the three offset stacks suggest that, even if we do not have offsets more than 3000 meters, it is still worthwhile to study anomalies with partial stacks. Their usefulness is further enhanced by the use of their complex attributes, which outline discontinuities and thin beds preferentially with frequency content. Since near-offset traces tend to have higher frequency content than mid-offset and far-offset traces, complex attributes are appropriate tools to be used in conjunction with other geophysical methods for analyzing partial stacks.

CURRENT RESEARCH

At present, the differences between full-wave equation modelling and ray-tracing modelling are being investigated. The emphasis is on the differences between the P-wave and S-wave synthetics of thin-bed models generated by the ray-tracing method and those generated by the full-wave equation method. In particular, AVO effects and complex attributes of these synthetics will be studied and compared. The results will also be compared to those generated by physical models. To generate synthetics, the Sierra ray-tracing modelling and full-wave equation modelling packages will be employed.

REFERENCES

- Ostrander, W.J., 1984, Plane-wave reflection coefficients for gas sands at non-normal angles of incidence: *Geophysics* v.49, 1637-1648.
- Robertson, J.D., Nogami, H.H., 1984, Complex seismic trace analysis of thin beds: *Geophysics*, v.49, p.344-352.
- Taner, M.T., Kochler, F., and Sheriff, R.E., 1979, Complex seismic trace analysis: *Geophysics*, v.44, p.1041-1063.
- Widess, M.B., 1973, How thin is a thin bed?: *Geophysics*, v.38, p.1176-1180.

ACKNOWLEDGEMENT

We thank Seis-pro Consultants Ltd. for providing excellent processing of the seismic line and offering many valuable suggestions during the development of the project. We also want to thank Alberta Energy Company and Summit Resources for allowing the use of one of their seismic lines. Special thanks are extended to Mr. Andrew Mah and Mr. Brian Doherty for organizing the various materials.

Glaucconitic Channel

- Geological Cross Section
- Channel
- Regional
- Seismic Template Line

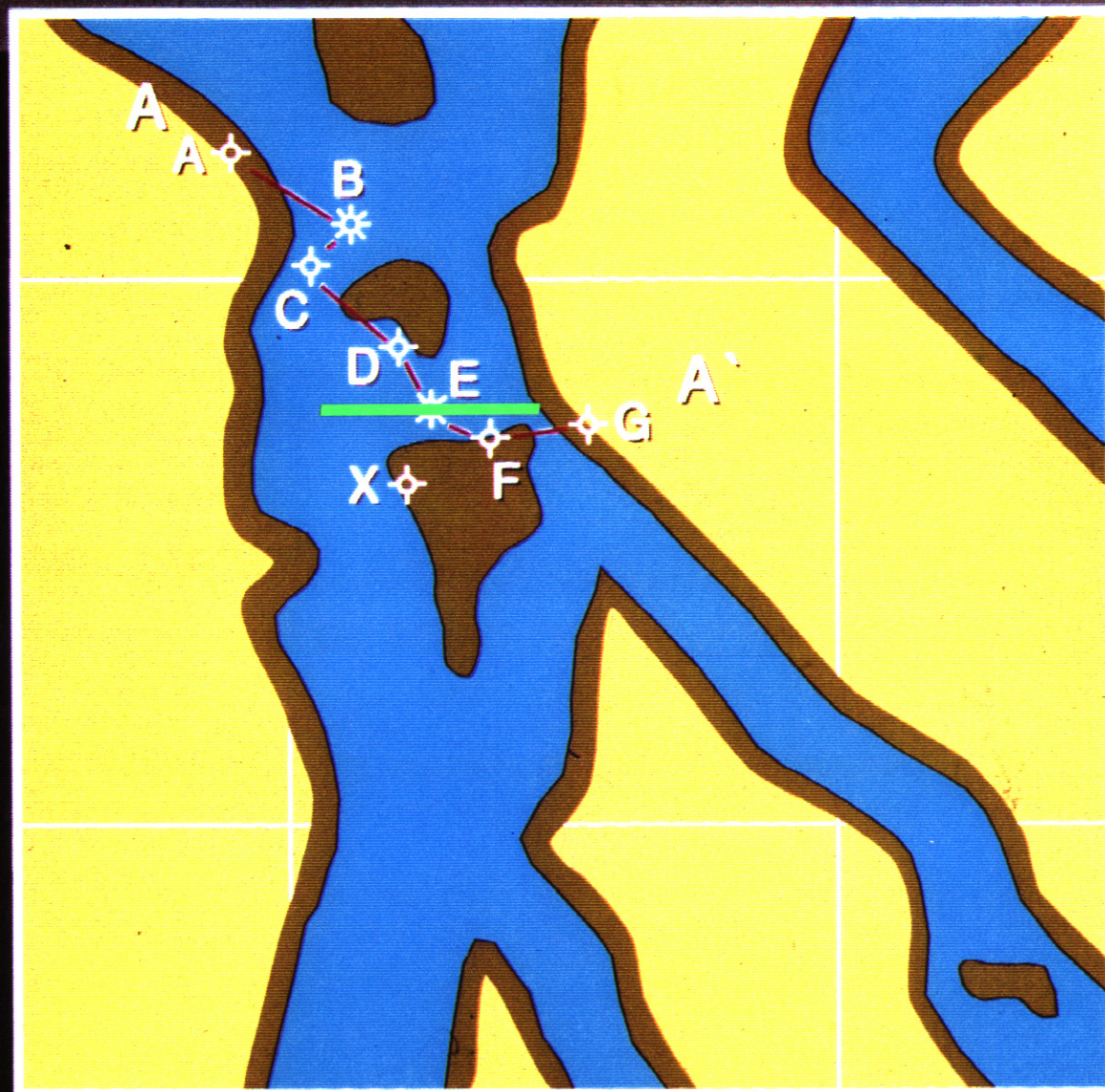


Figure 1. Interpreted Glauconite channels

Glaucconitic Channel

Structural Cross Section

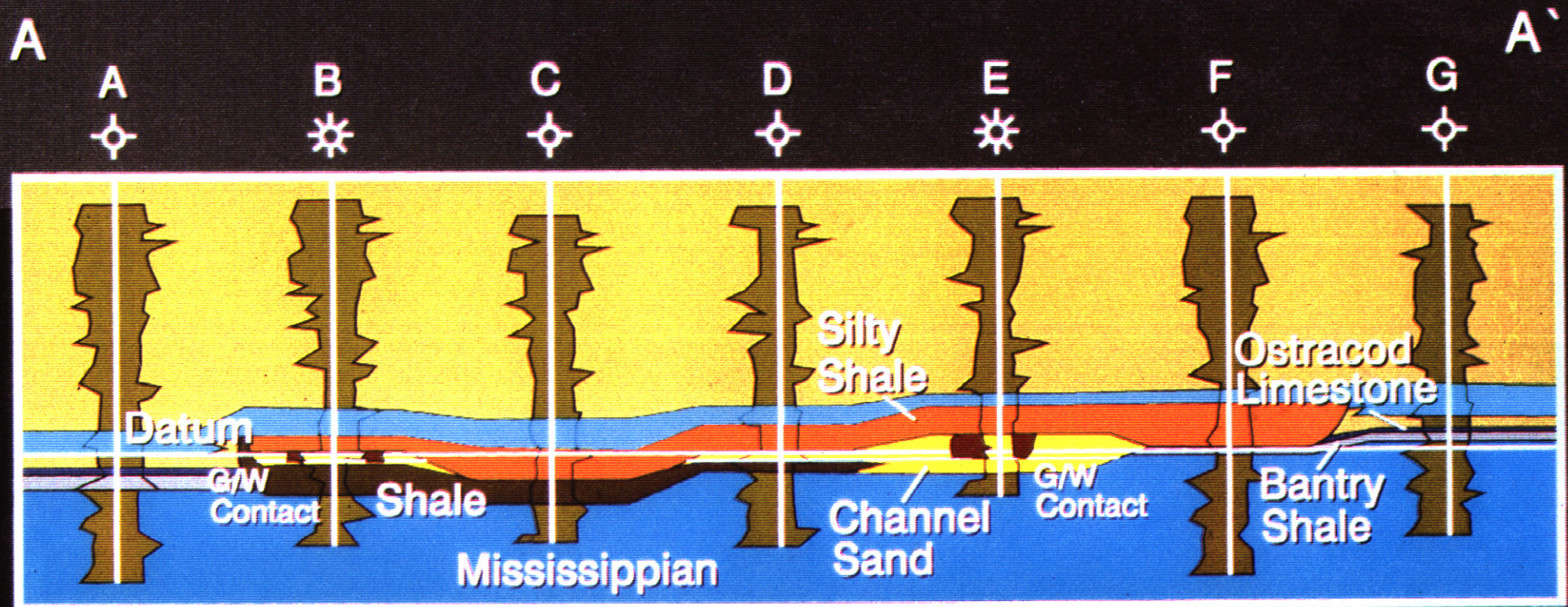
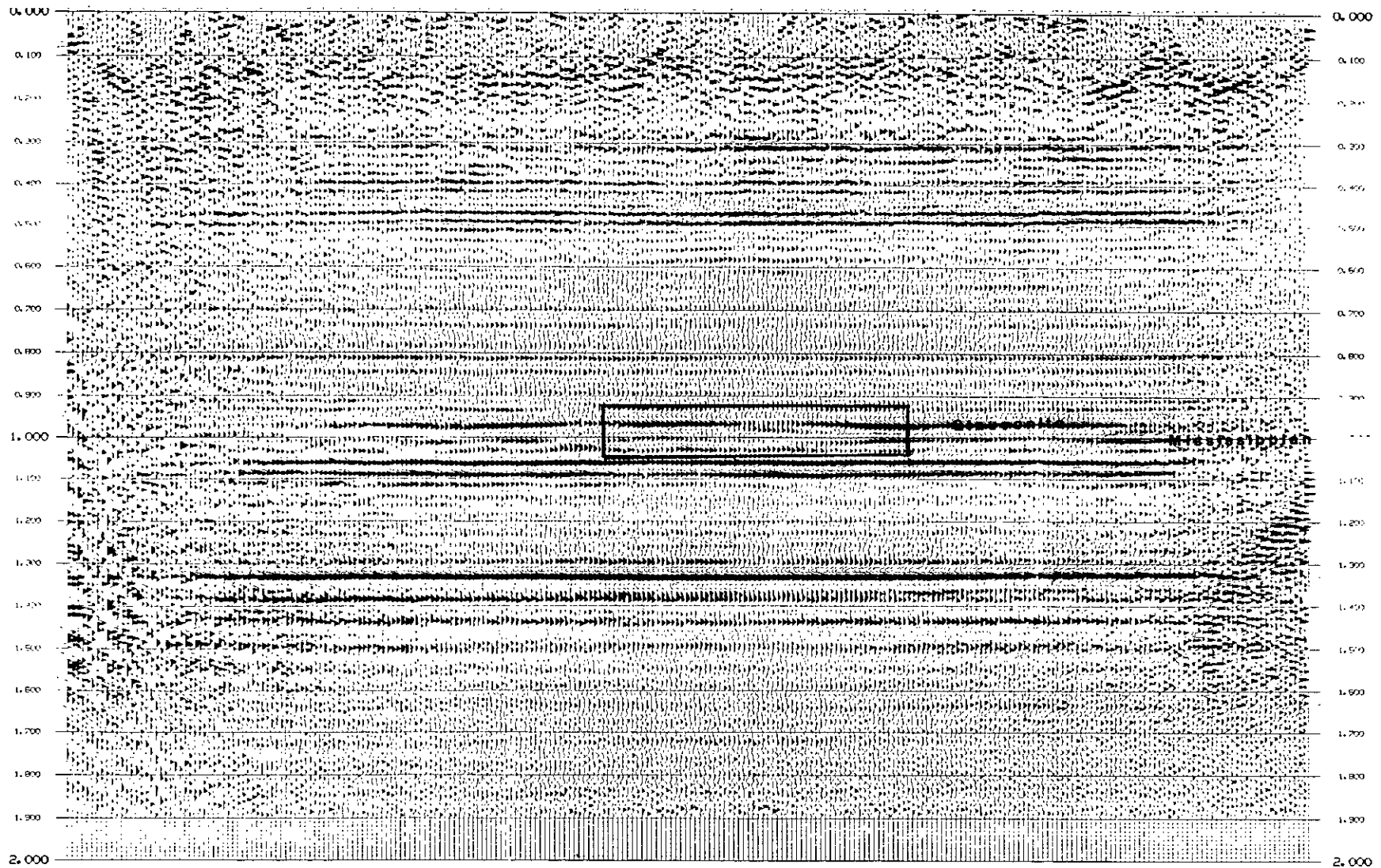
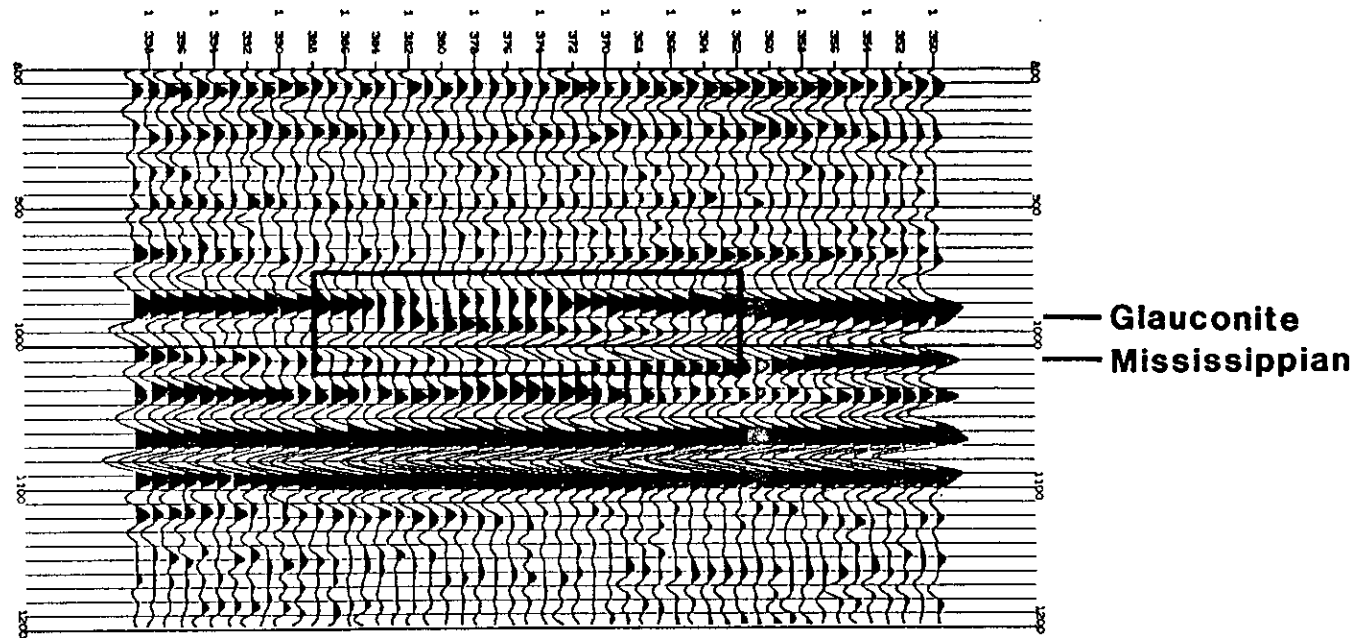


Figure 2. Structural cross section AA' (figure 1)



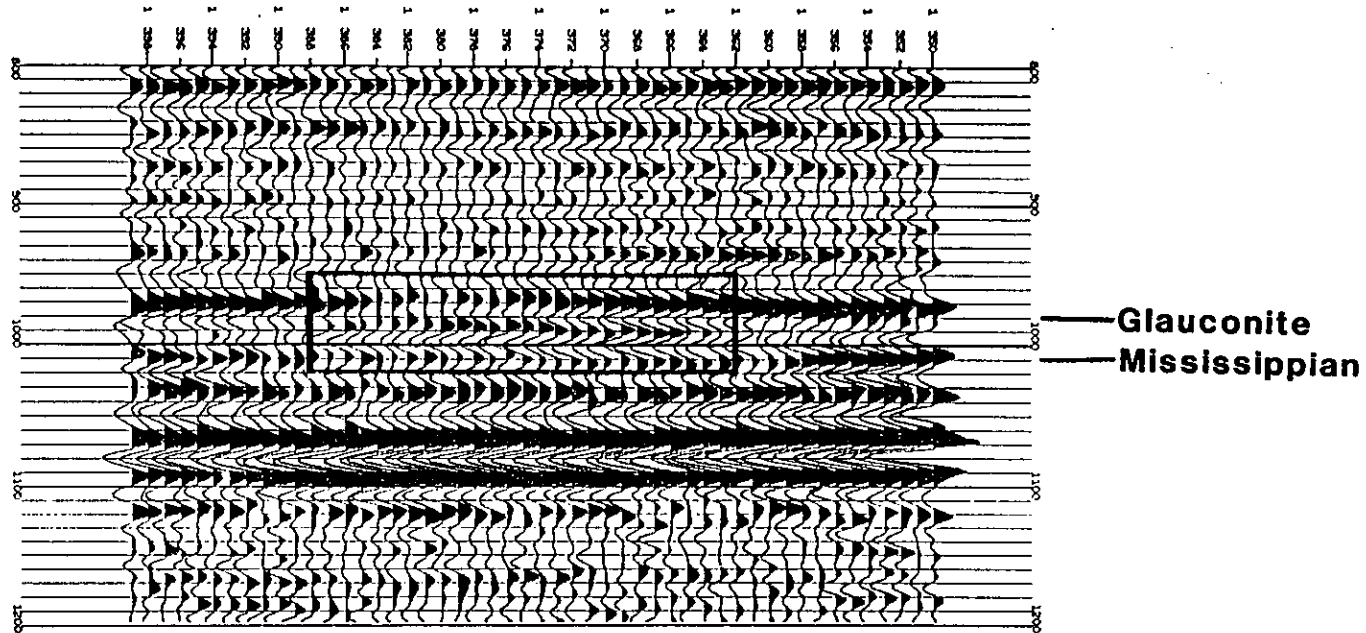
**Figure 3. Final full-offset stack of seismic template line
Gas sandbar is boxed in**



full-offset stack

0-2100 meters

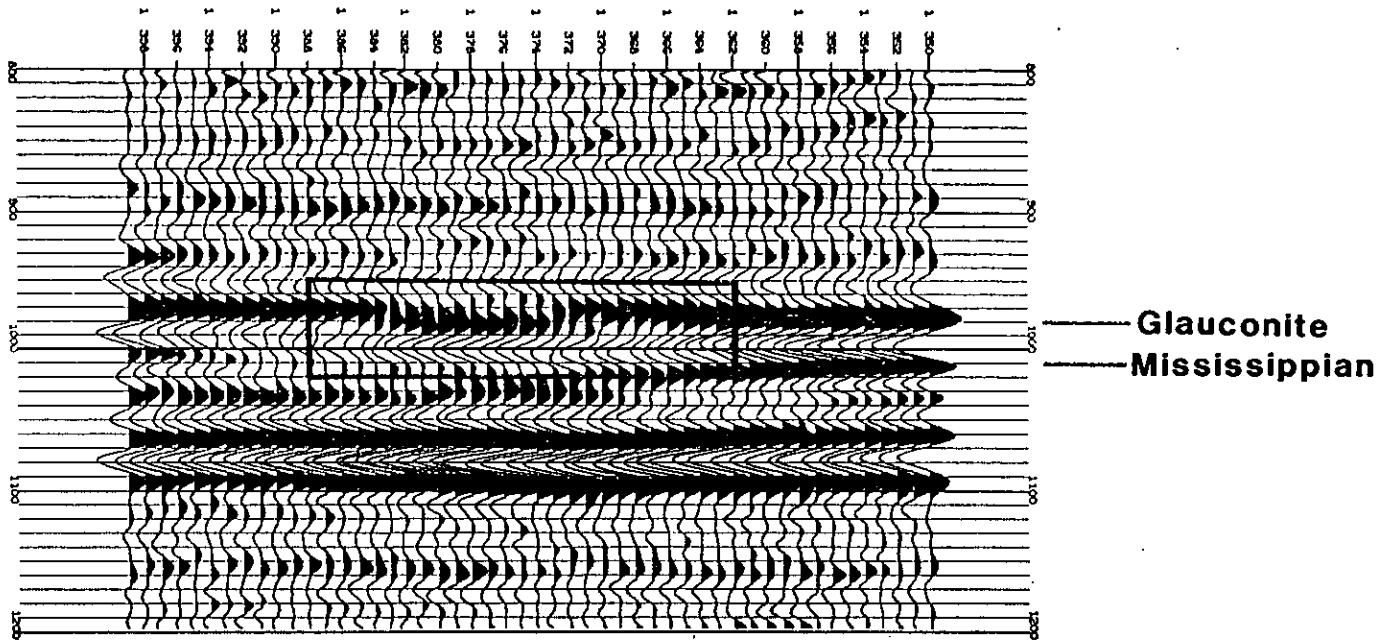
Figure 4. Full-offset stack of template seismic anomaly, normal polarity.



near-offset stack

0-1050 meters

Figure 5. Near-offset stack of template seismic anomaly, normal polarity



mid-offset stack

1050-2100 meters

Figure 6. Mid-offset stack of template seismic anomaly, normal polarity

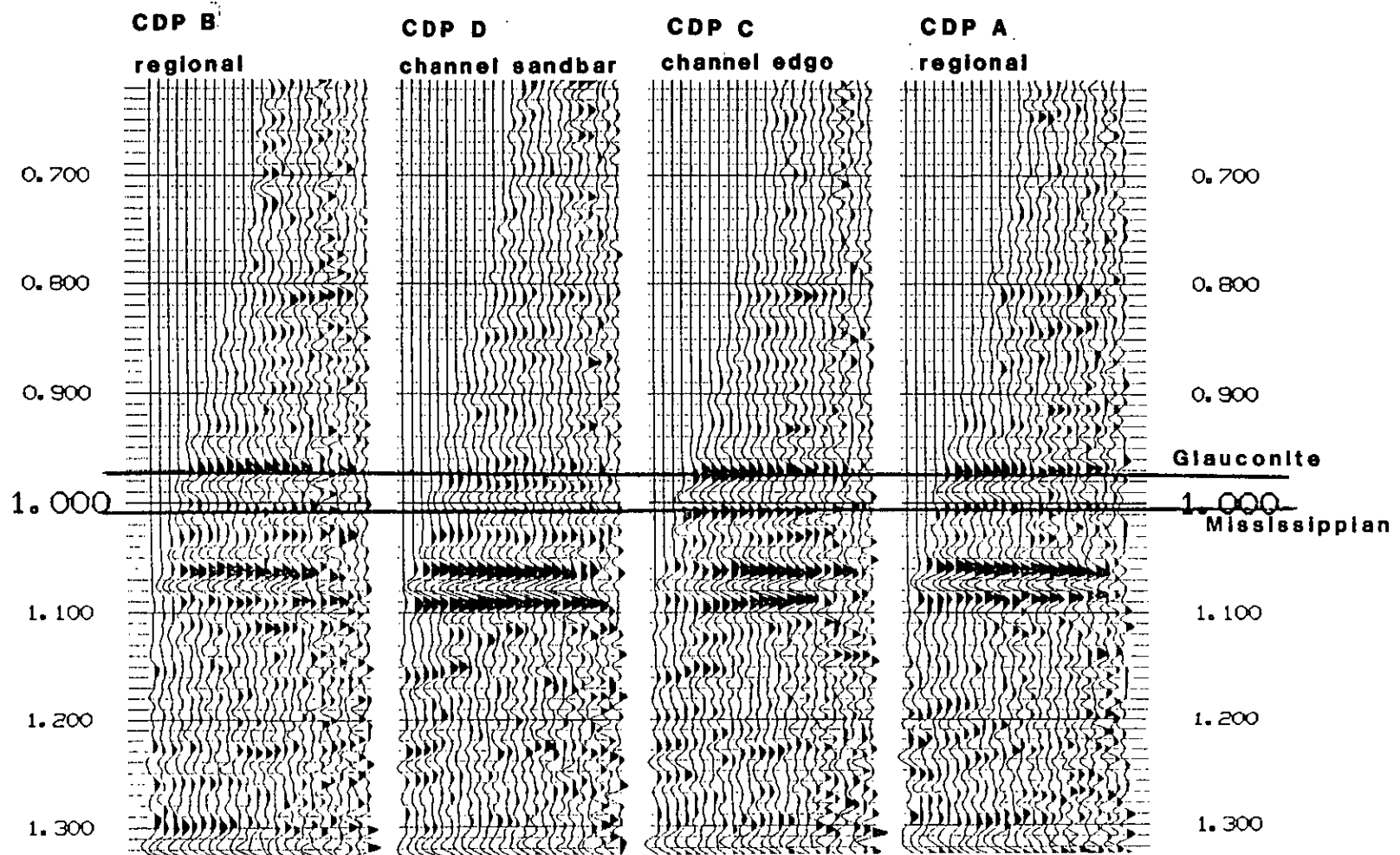
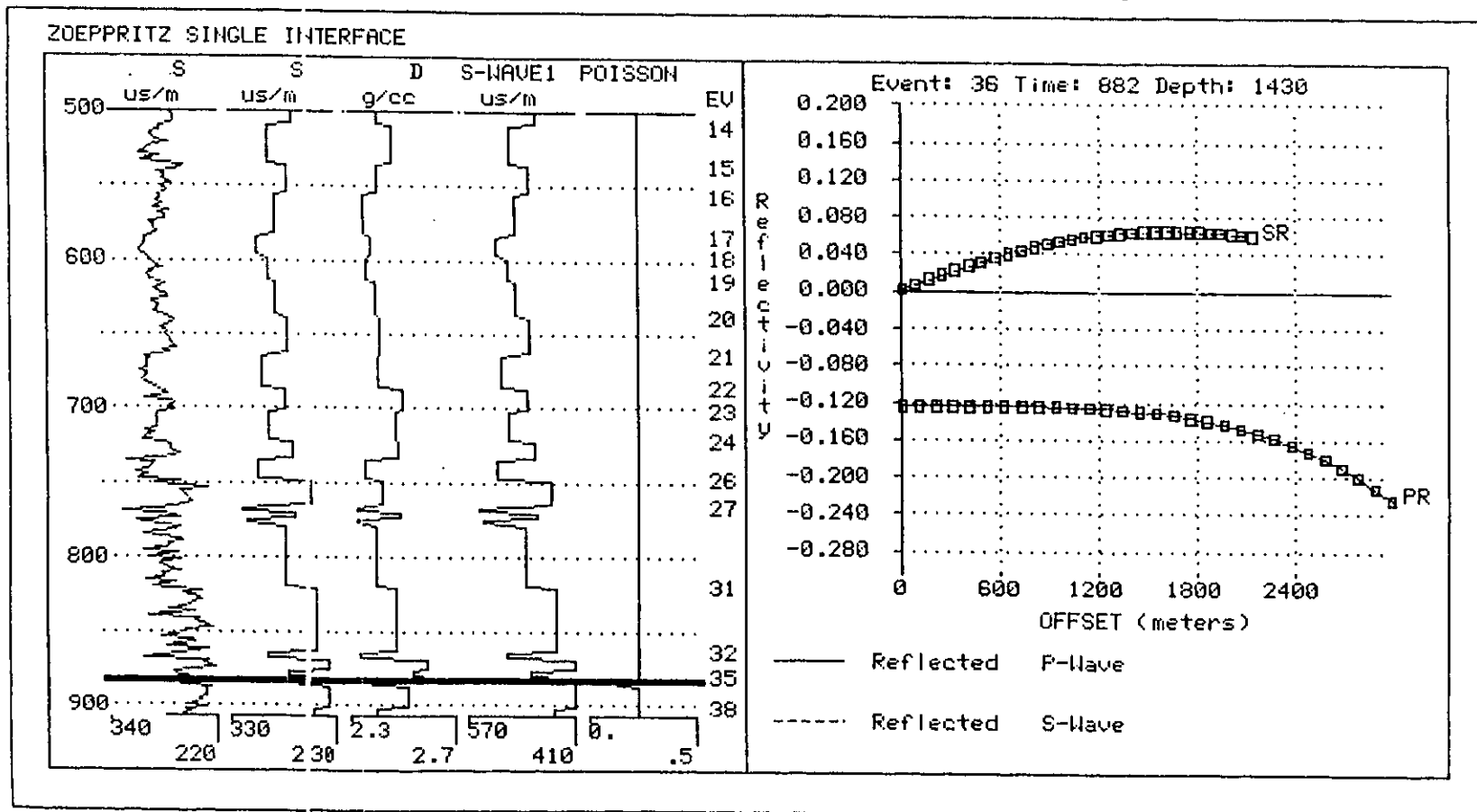


Figure 7. Ostrander gather, summing over six CDP locations and three-offset range with trace-balancing, normal polarity

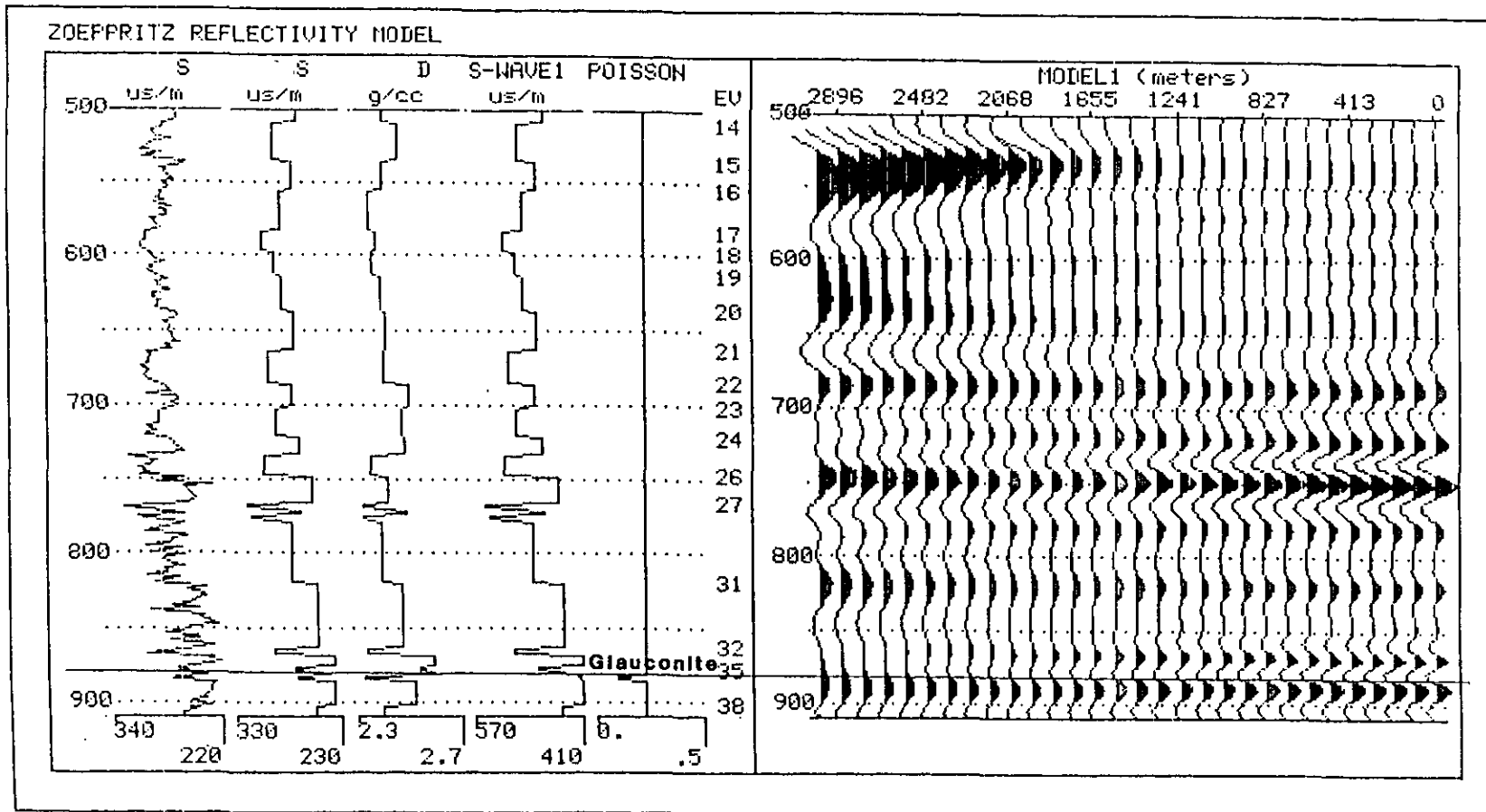
channel gas well, 8 meters sand, Poisson's ratio 0.1



306

Figure 8a. Reflection coefficients versus offsets for the Glauconite Formation in modified well (B)

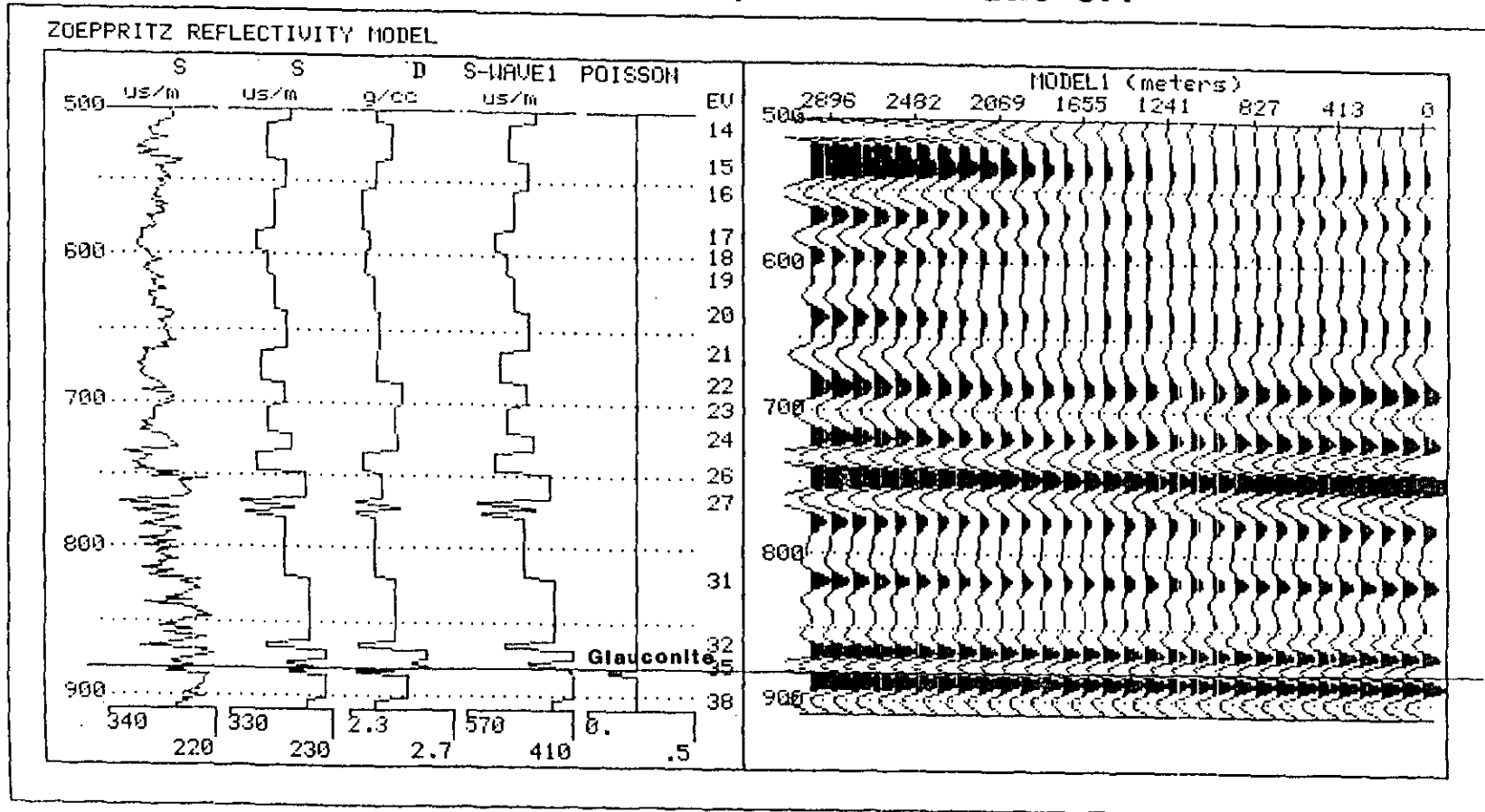
channel gas well, 8 meters sand, Poisson's ratio 0.1



307

Figure 8b. NMO corrected synthetic for modified well (B)

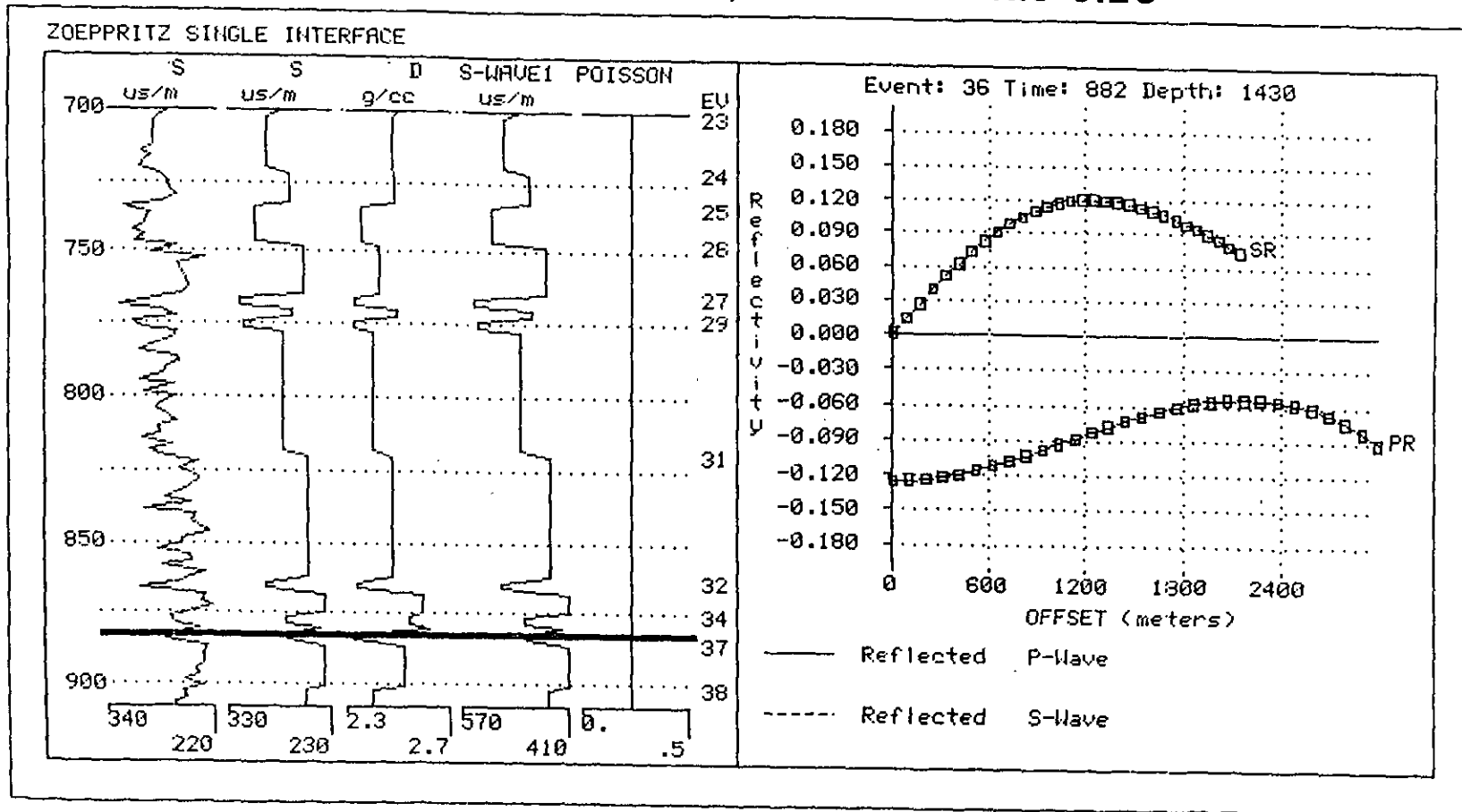
channel gas well, 8 meters sand, Poisson's ratio 0.1



308

Figure 8c. Plane-wave solution synthetic for modified well (B)

channel gas well, 8 meters sand, Poisson's ratio 0.25



309

Figure 9a. Reflection coefficients versus offsets for the Glauconite Formation in modified well (B)

channel gas well, 8 meters sand, Poisson's ratio 0.25

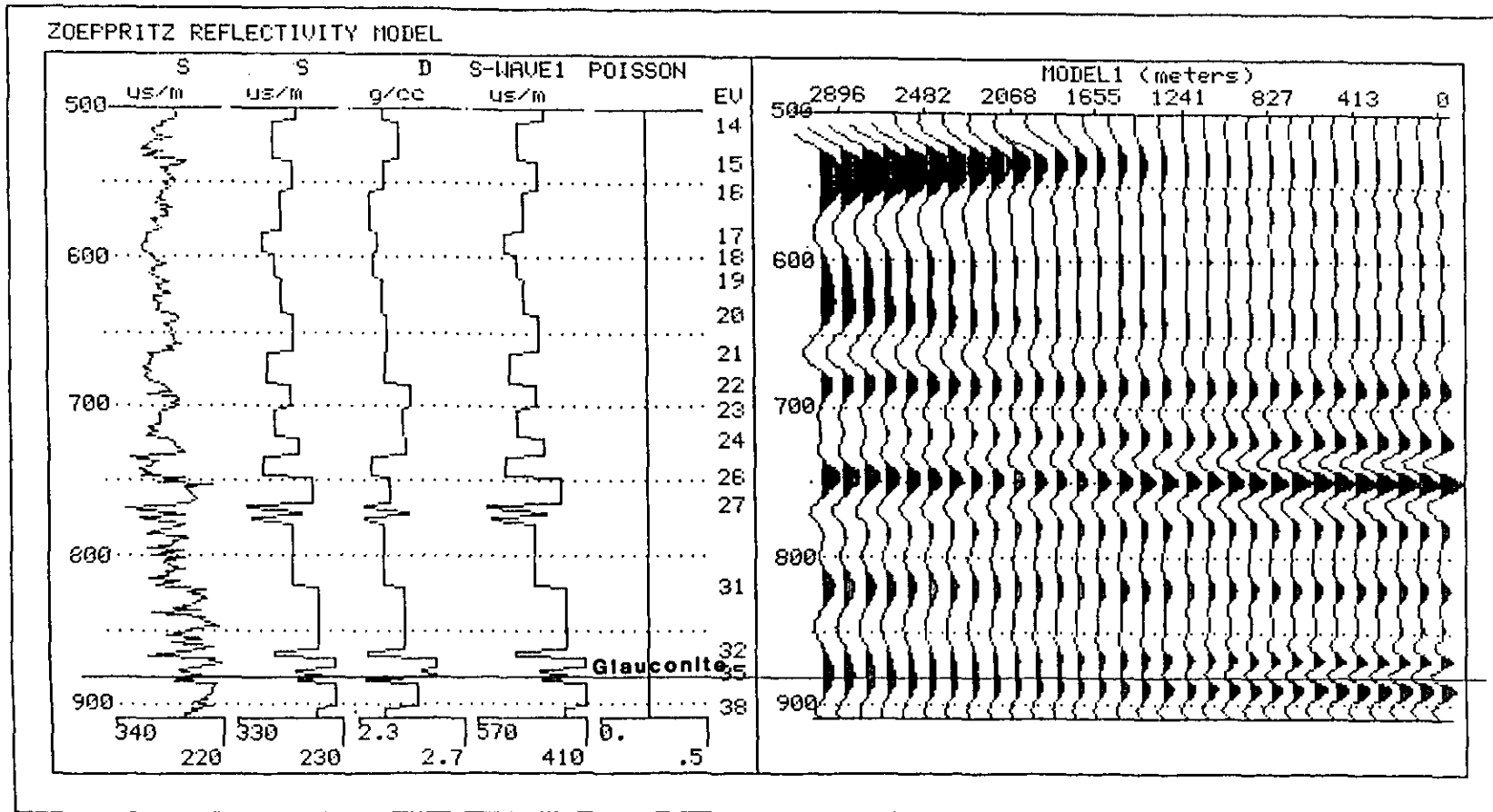
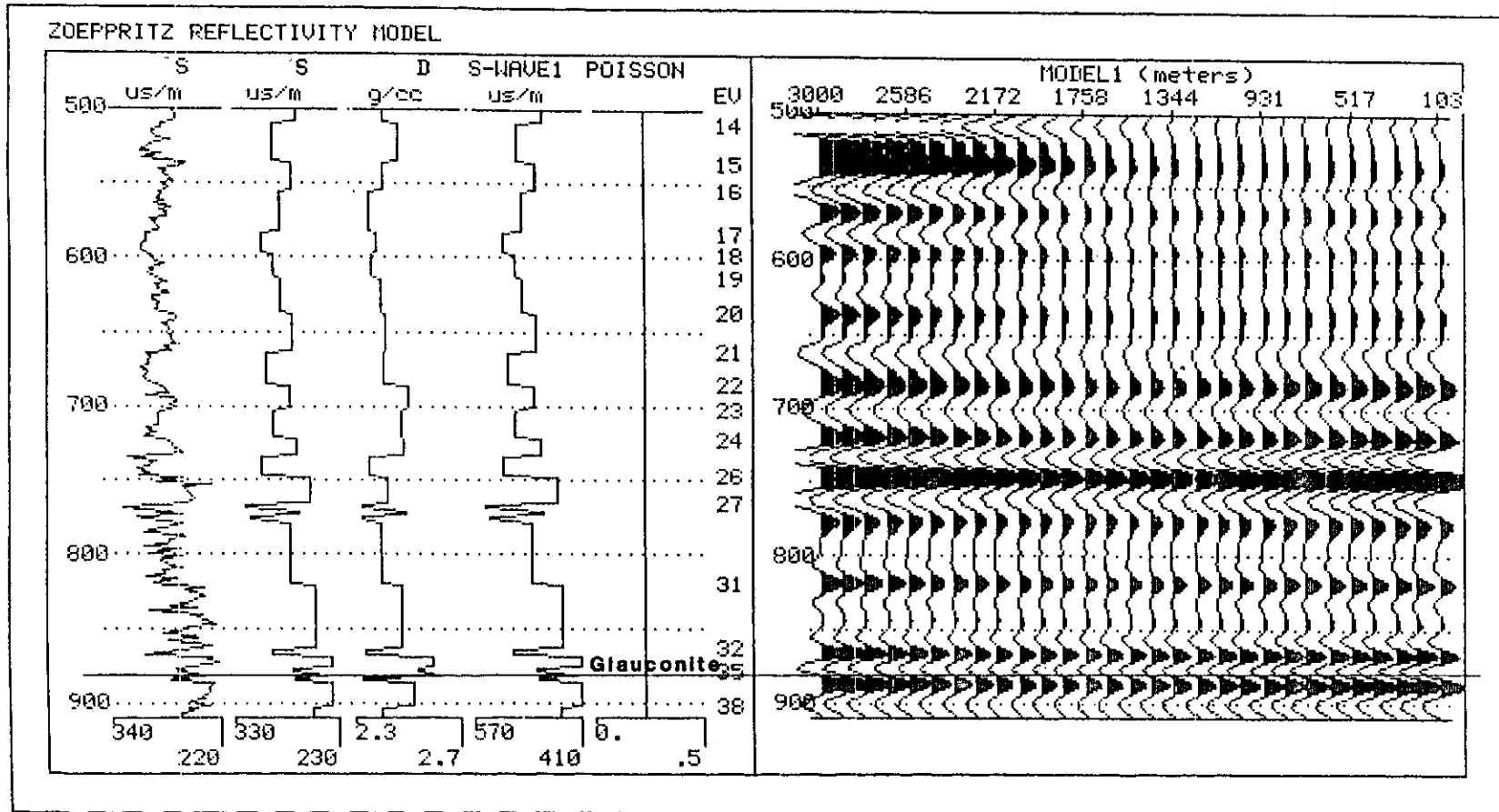


Figure 9b. NMO corrected synthetic for modified well (B)

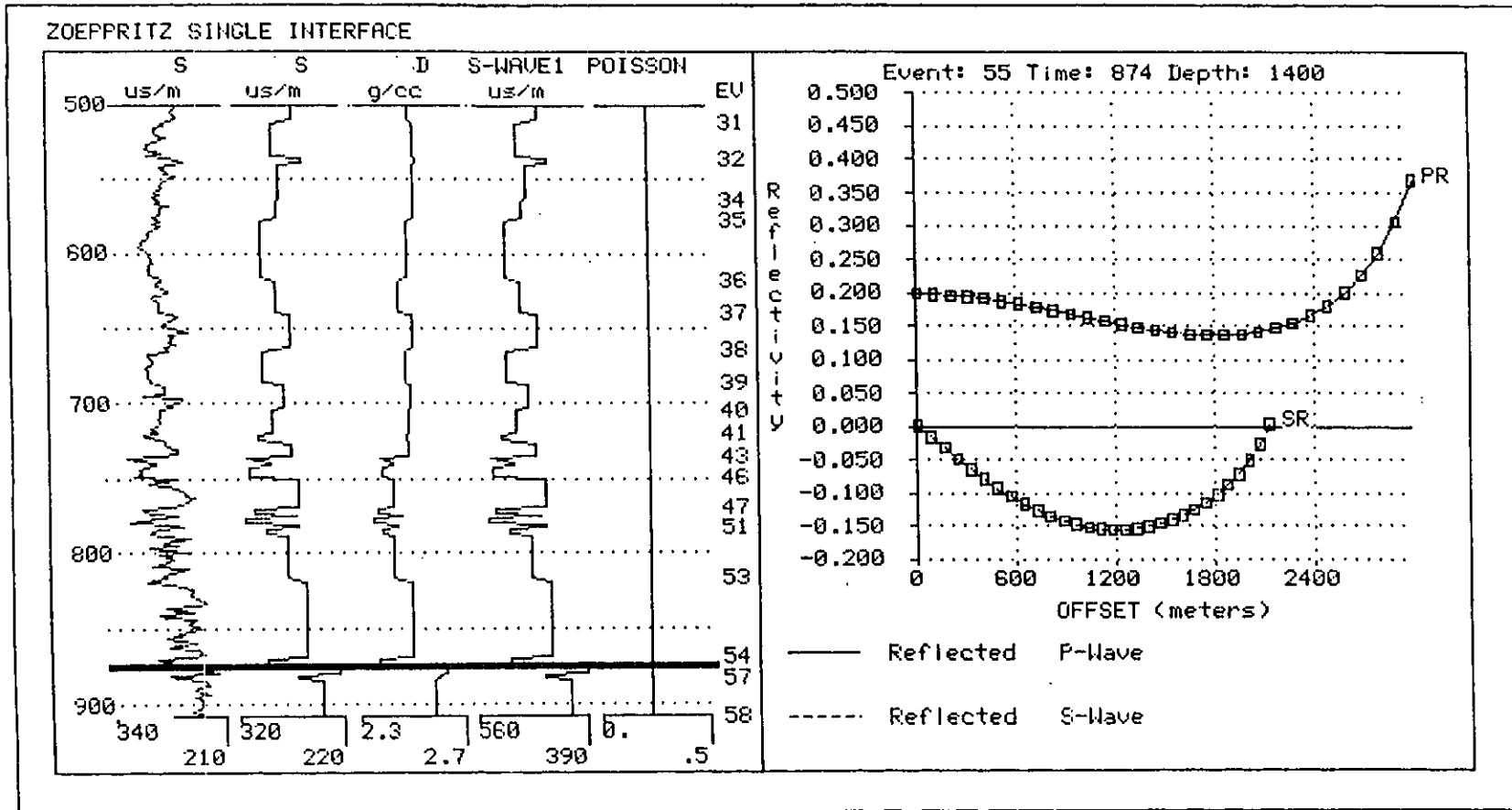
channel gas well, 8 meters sand, Poisson's ratio 0.25



311

Figure 9c. Plane-wave solution synthetic for modified well (B)

channel shale well



312

Figure 10a. Reflection coefficients versus offsets for the Glauconite Formation in channel shale well (C)

channel shale well

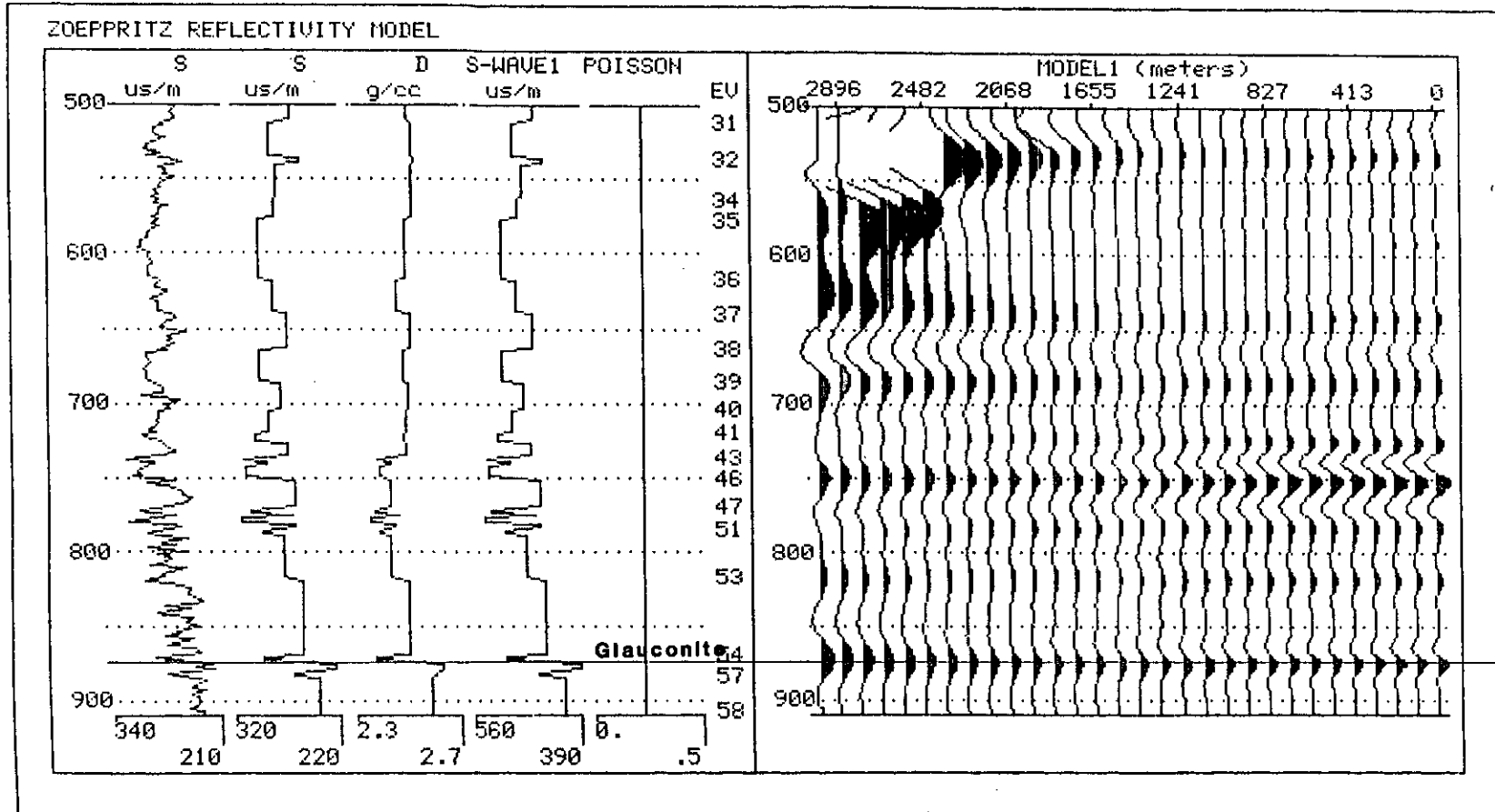
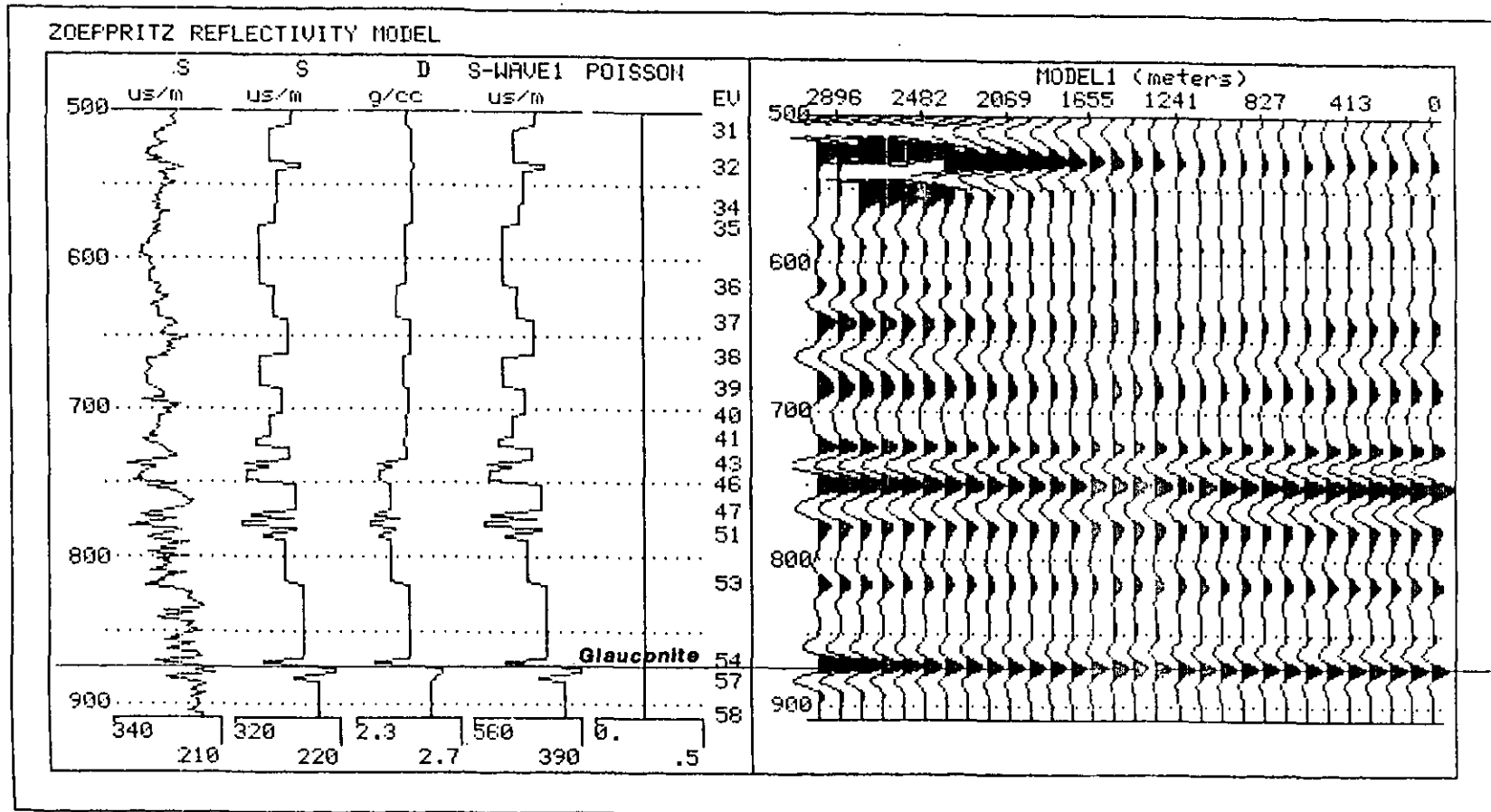


Figure 10b. NMO corrected synthetic for well (C)

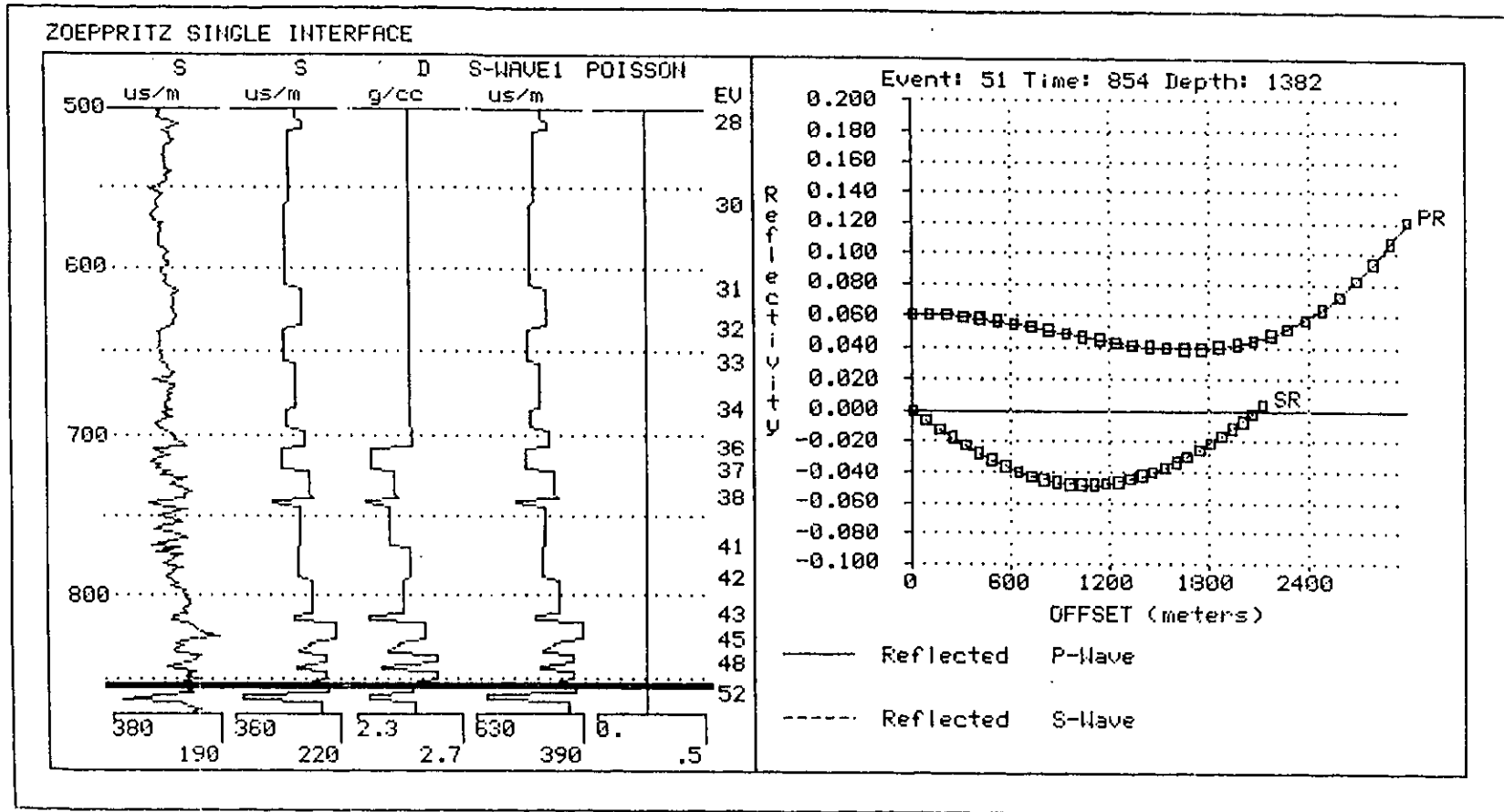
channel shale well



314

Figure 10c. Plane-wave solution synthetic for well (C)

regional well



315

Figure 11a. Reflection coefficients versus offsets for the Glauconite Formation in regional well (F)

regional well

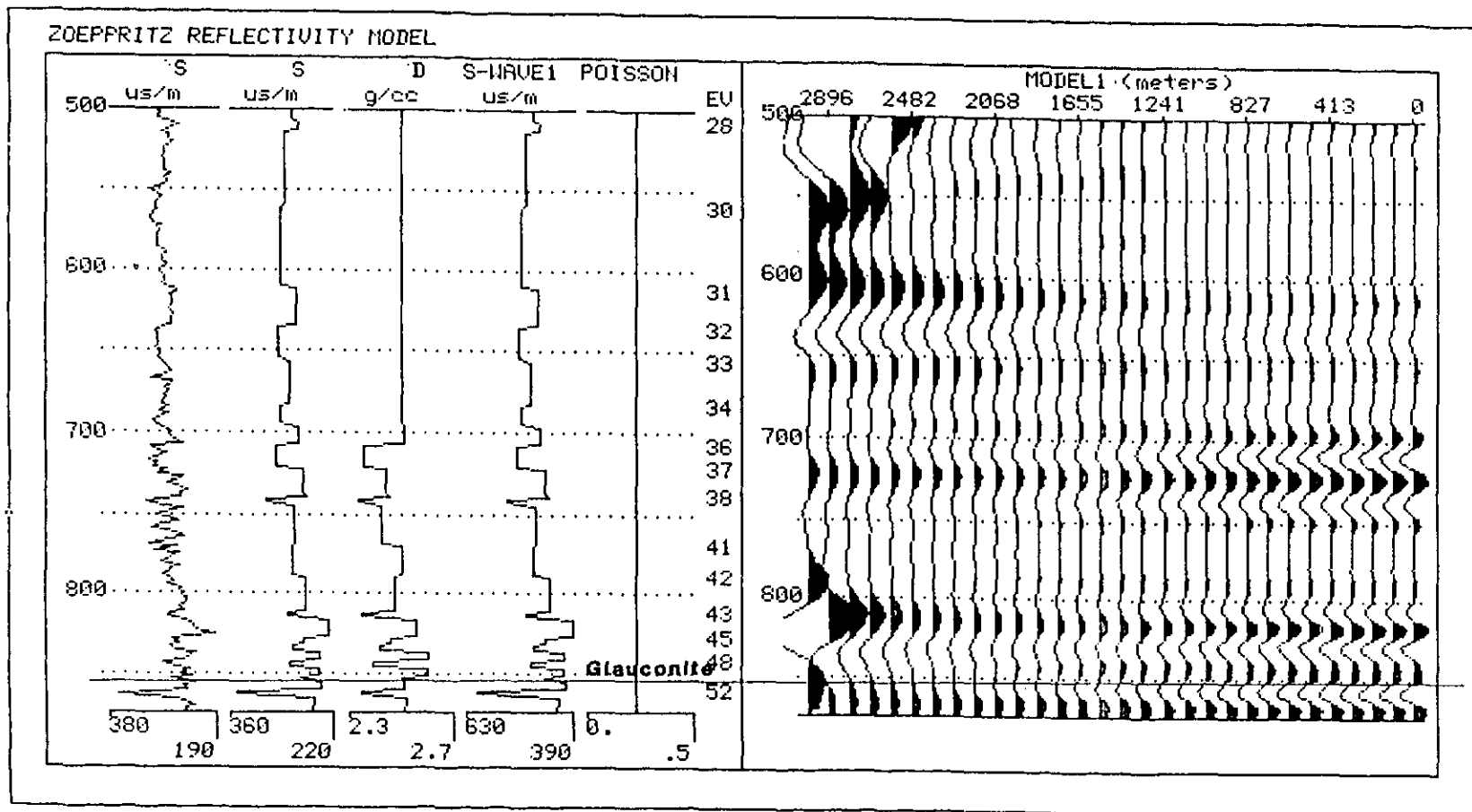


Figure 11b. NMO corrected synthetic for well (F)

regional well

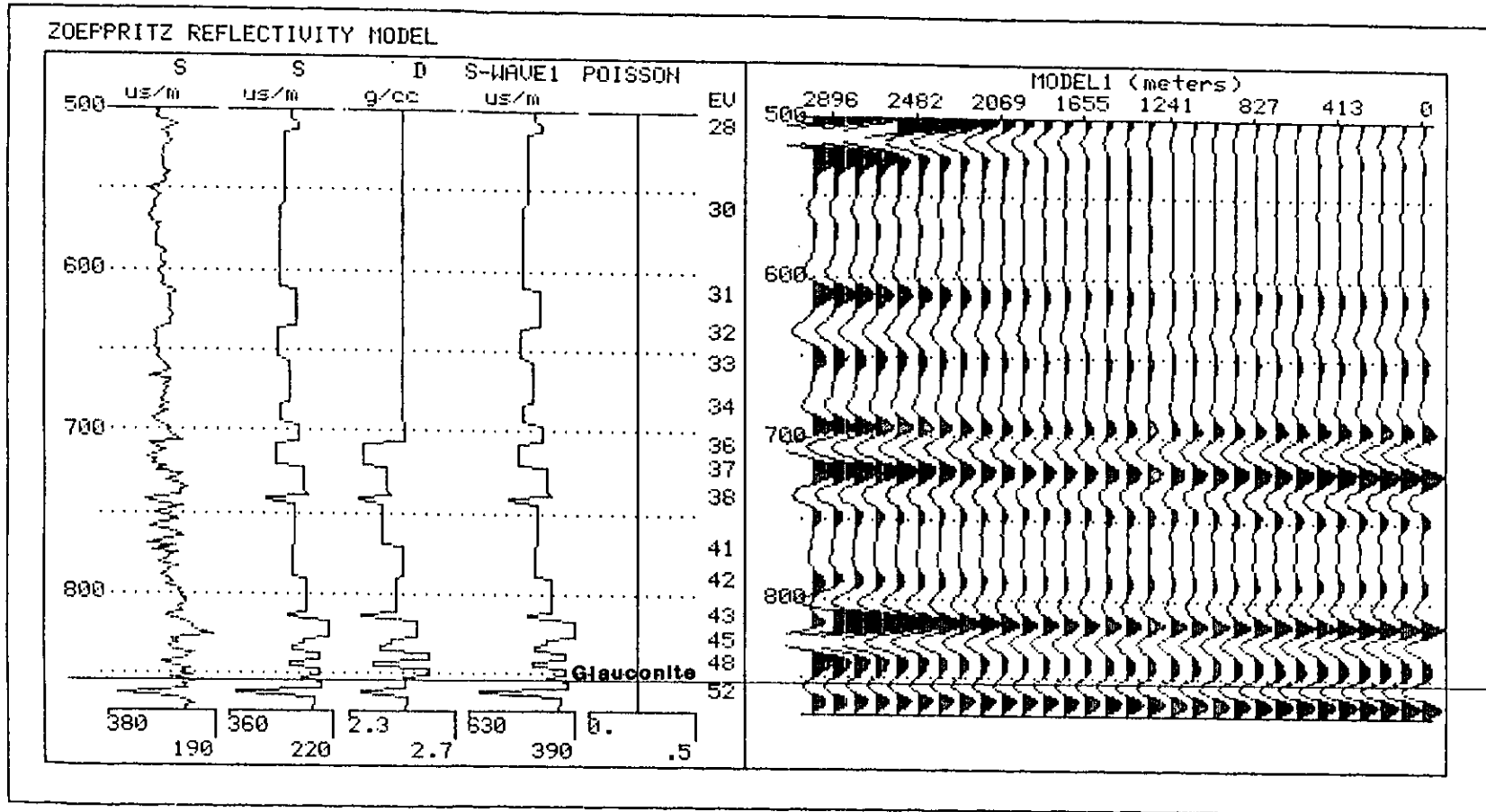
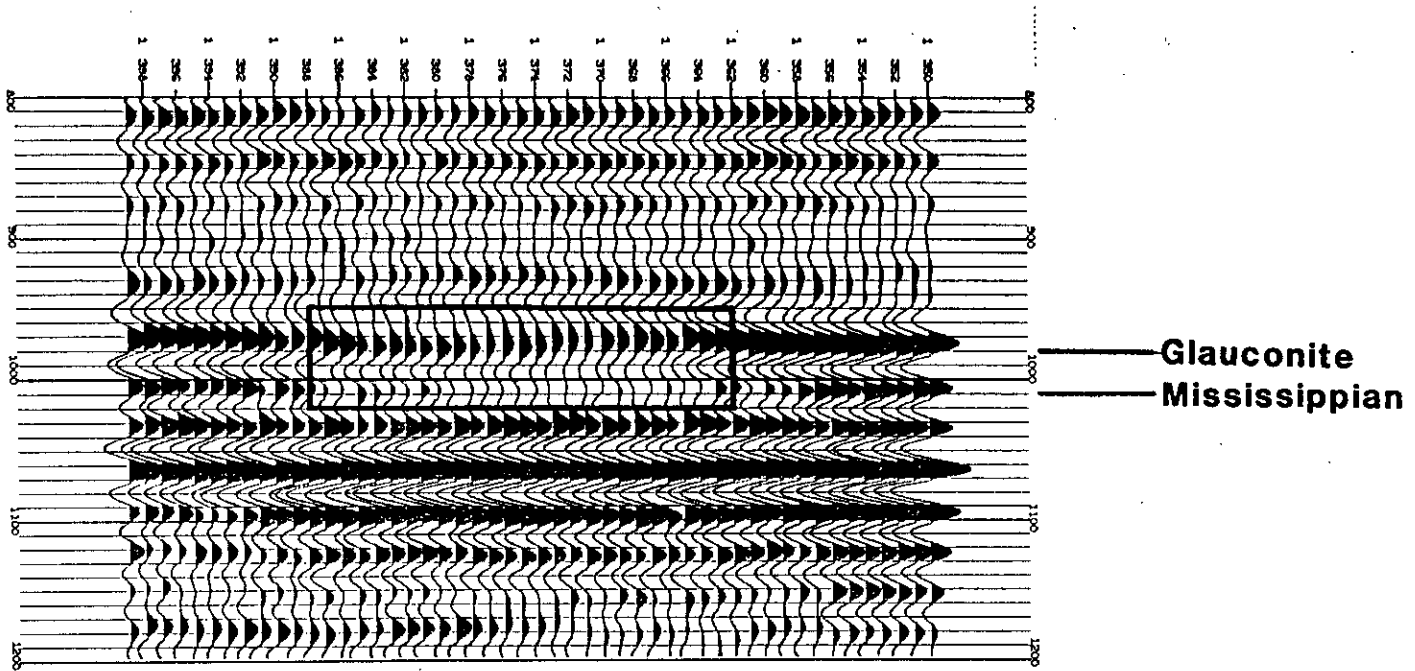
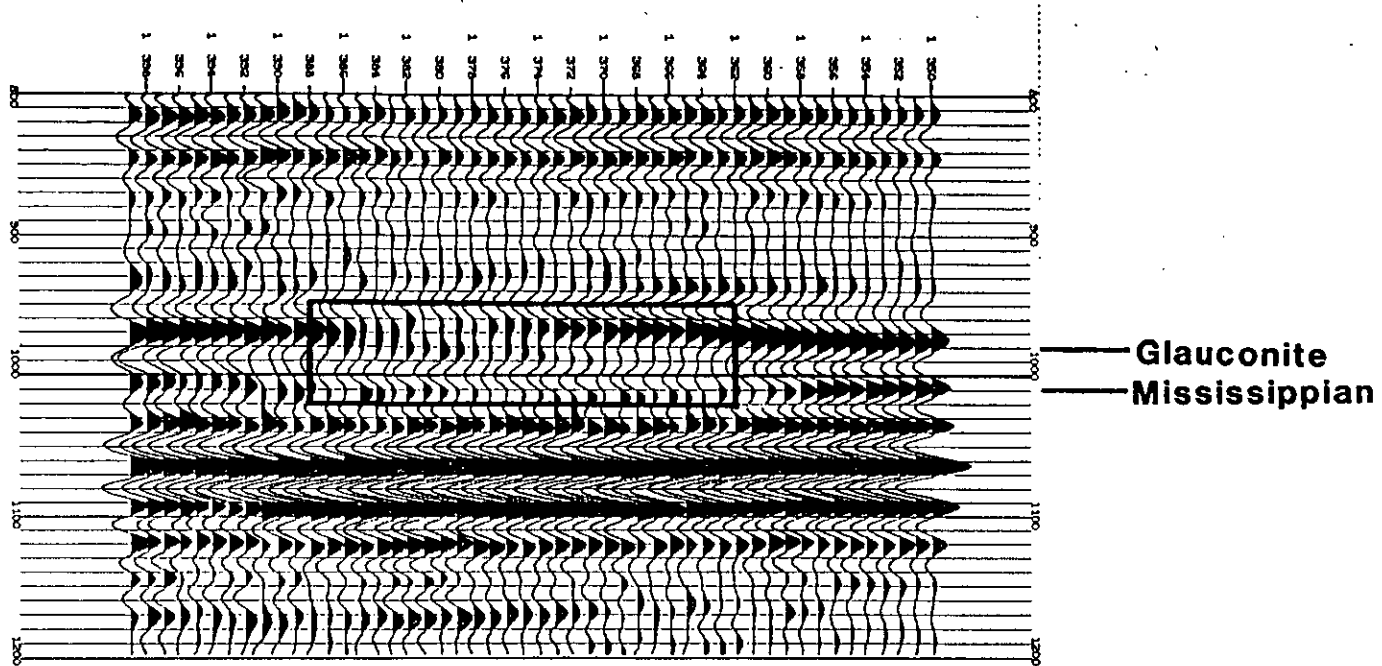


Figure 11c. Plane-wave solution synthetic for well (F)



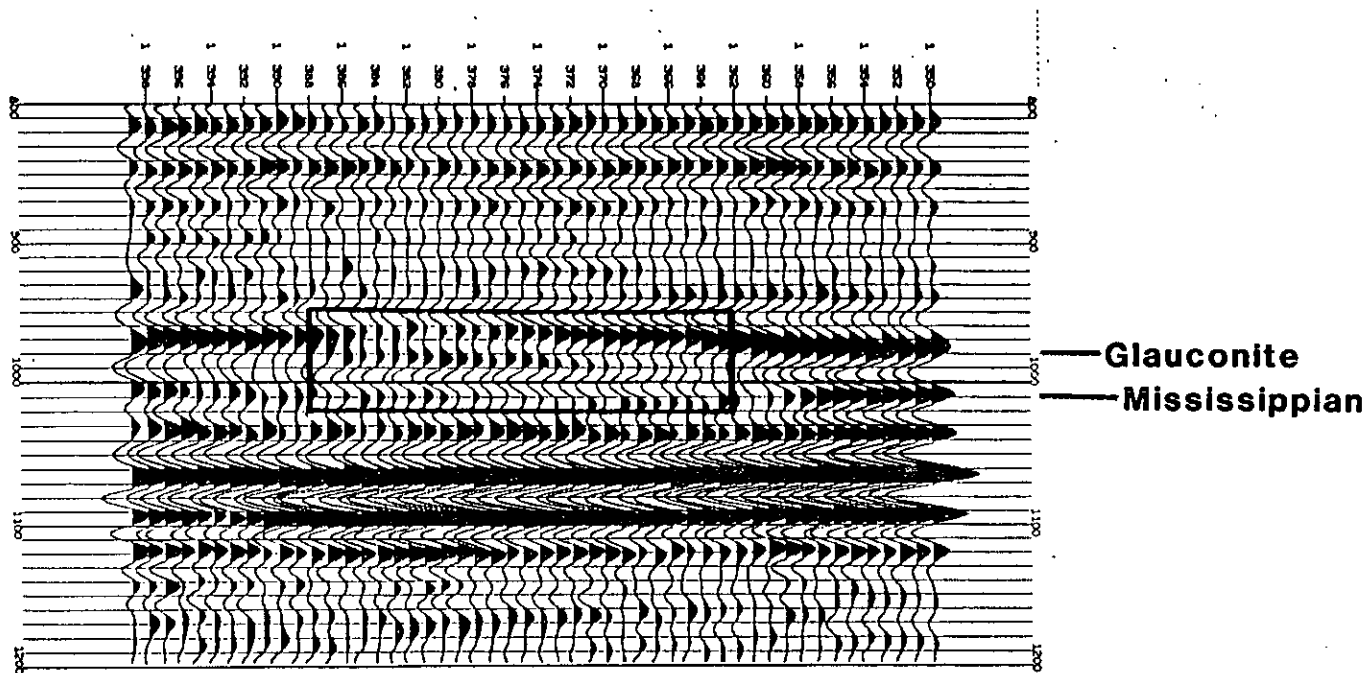
near-offset stack
8/16-35/40 Hz

Figure 12. Filtered near-offset stack



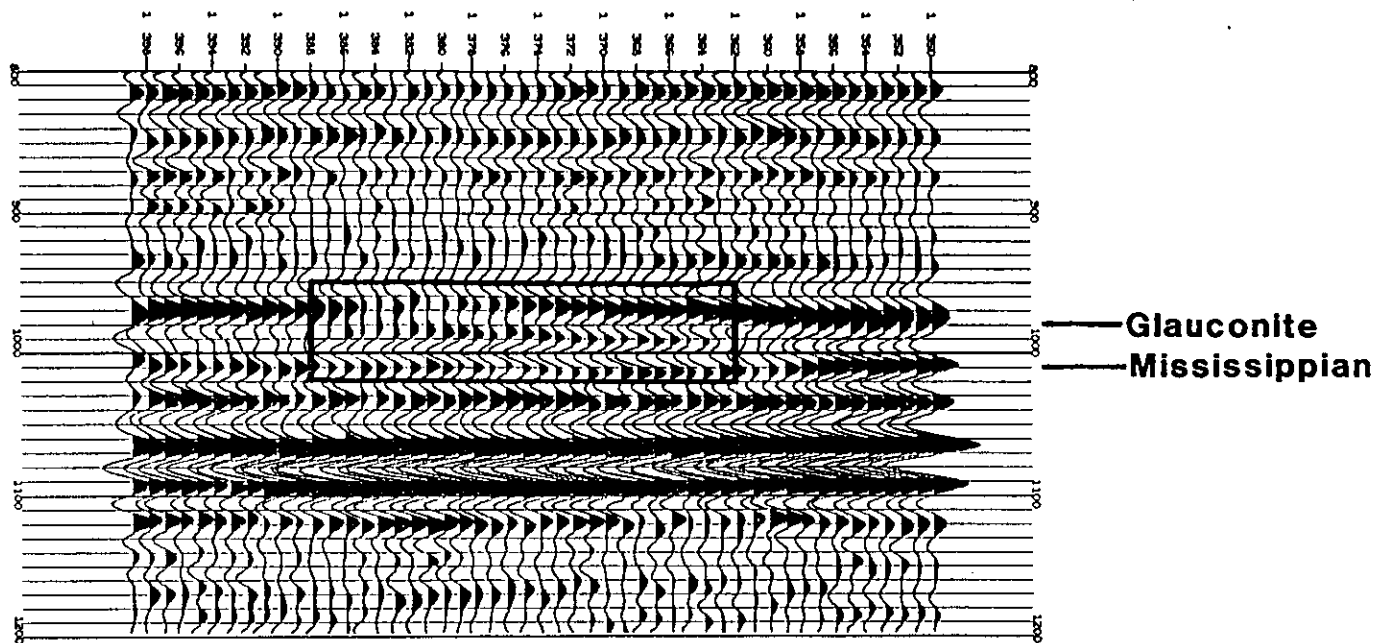
near-offset stack
8/16-40/45 Hz

Figure 13. Filtered near-offset stack



near-offset stack
8/16-45/50 Hz

Figure 14. Filtered near-offset stack



near-offset stack

8/16-50/55 Hz

Figure 15. Filtered near-offset stack

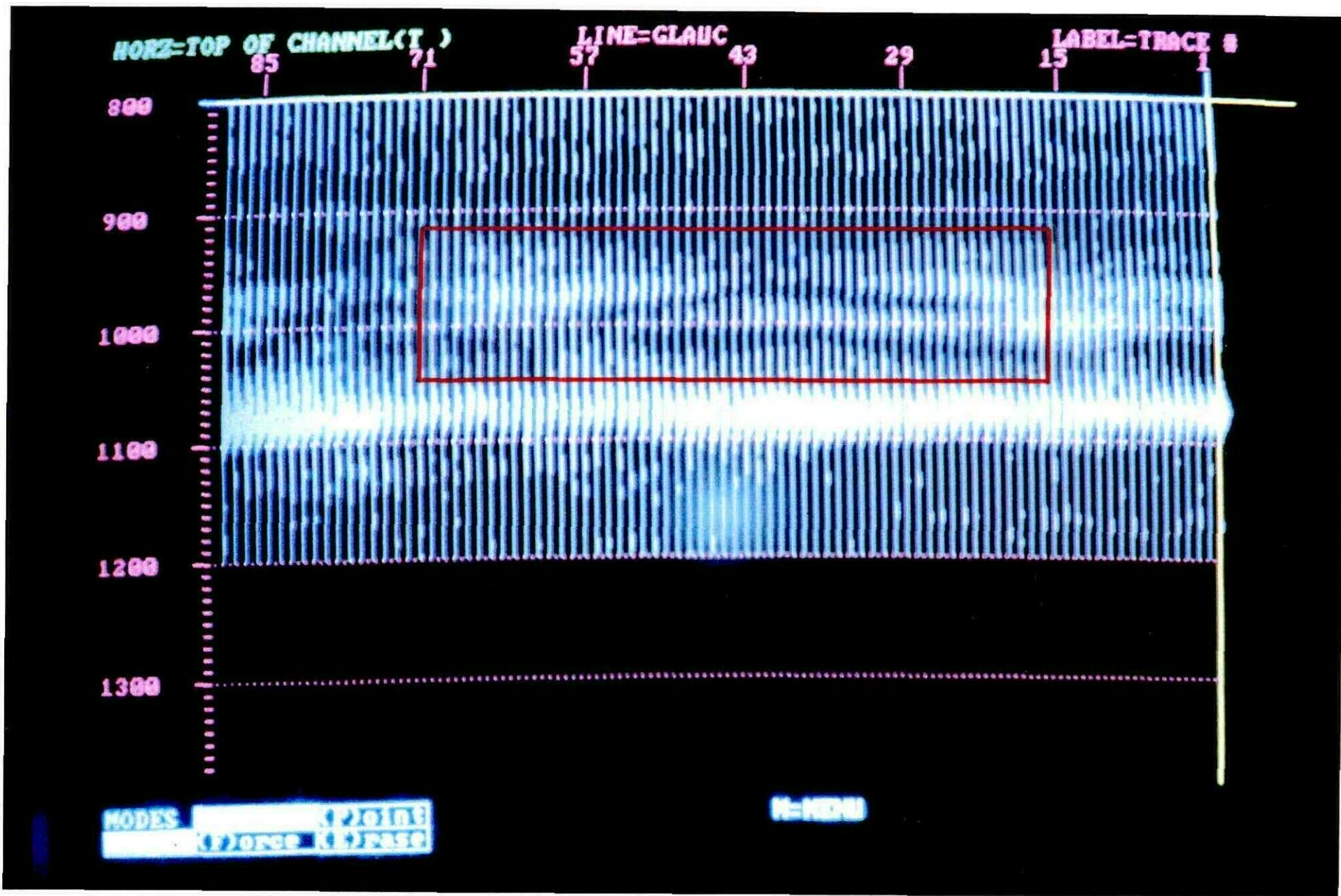


Figure 16. The instantaneous amplitude plot for the full-offset stack.

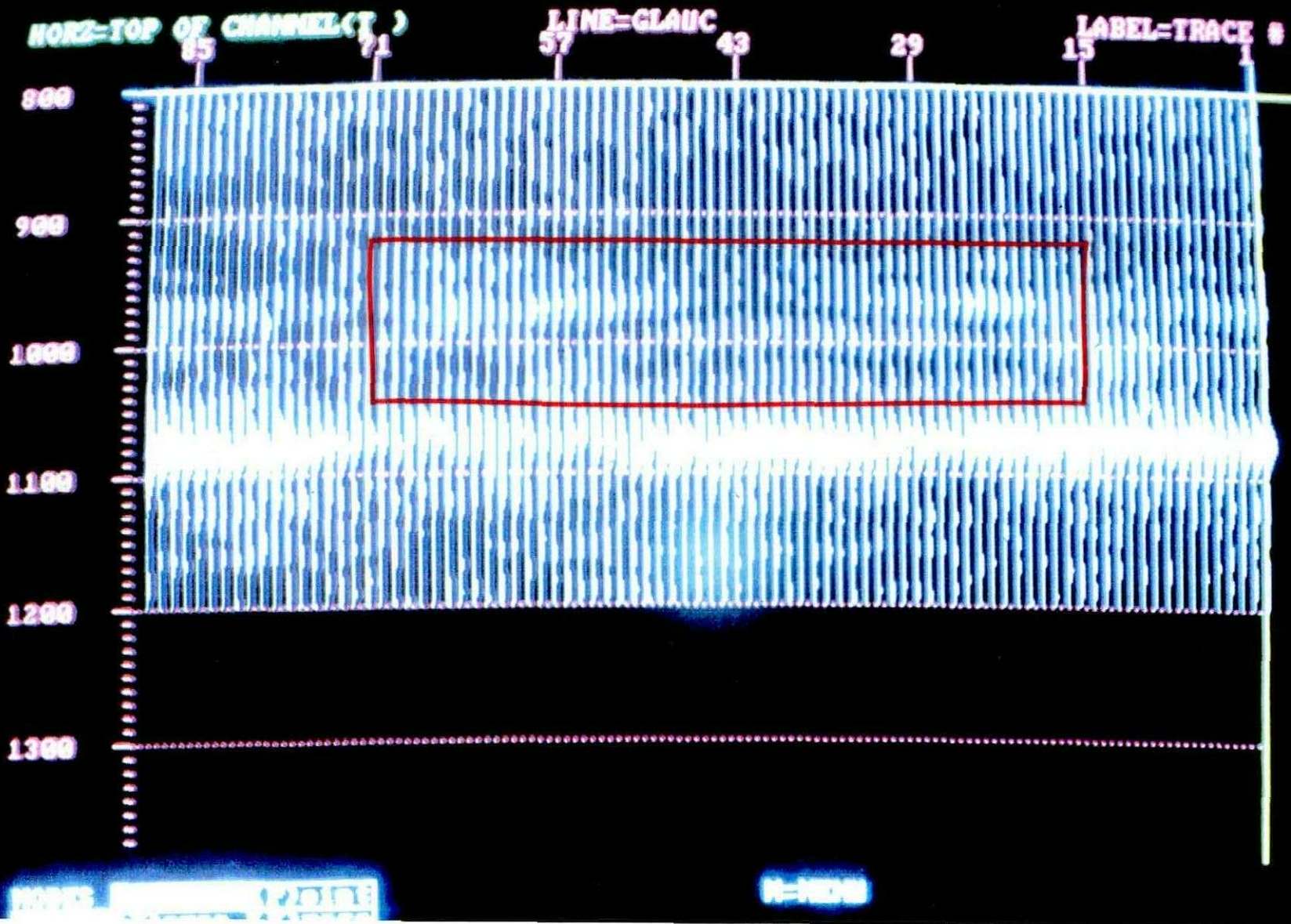


Figure 17. The instantaneous amplitude plot for the near-offset stack.

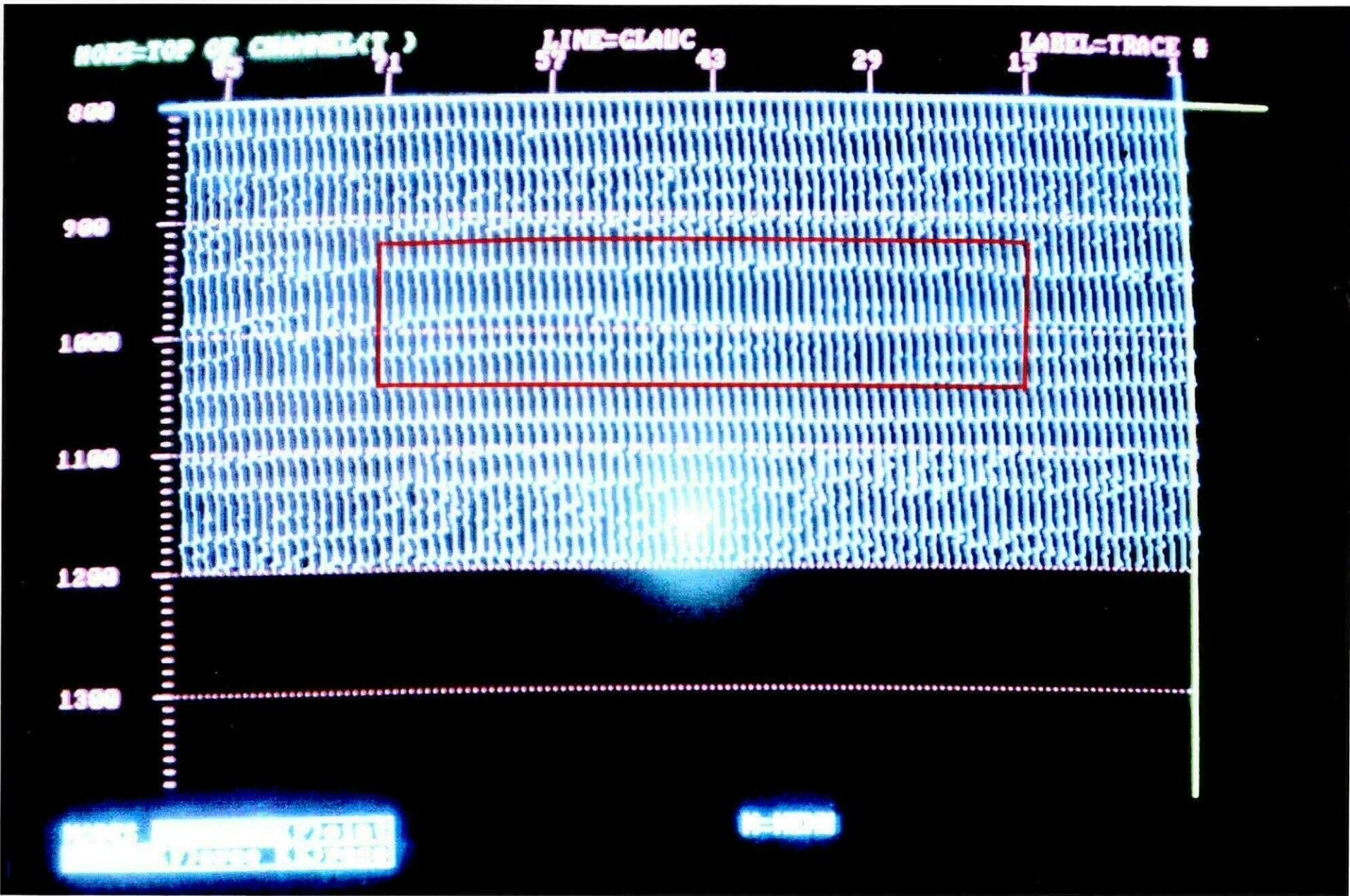


Figure 19. The instantaneous phase plot for the full-offset stack.

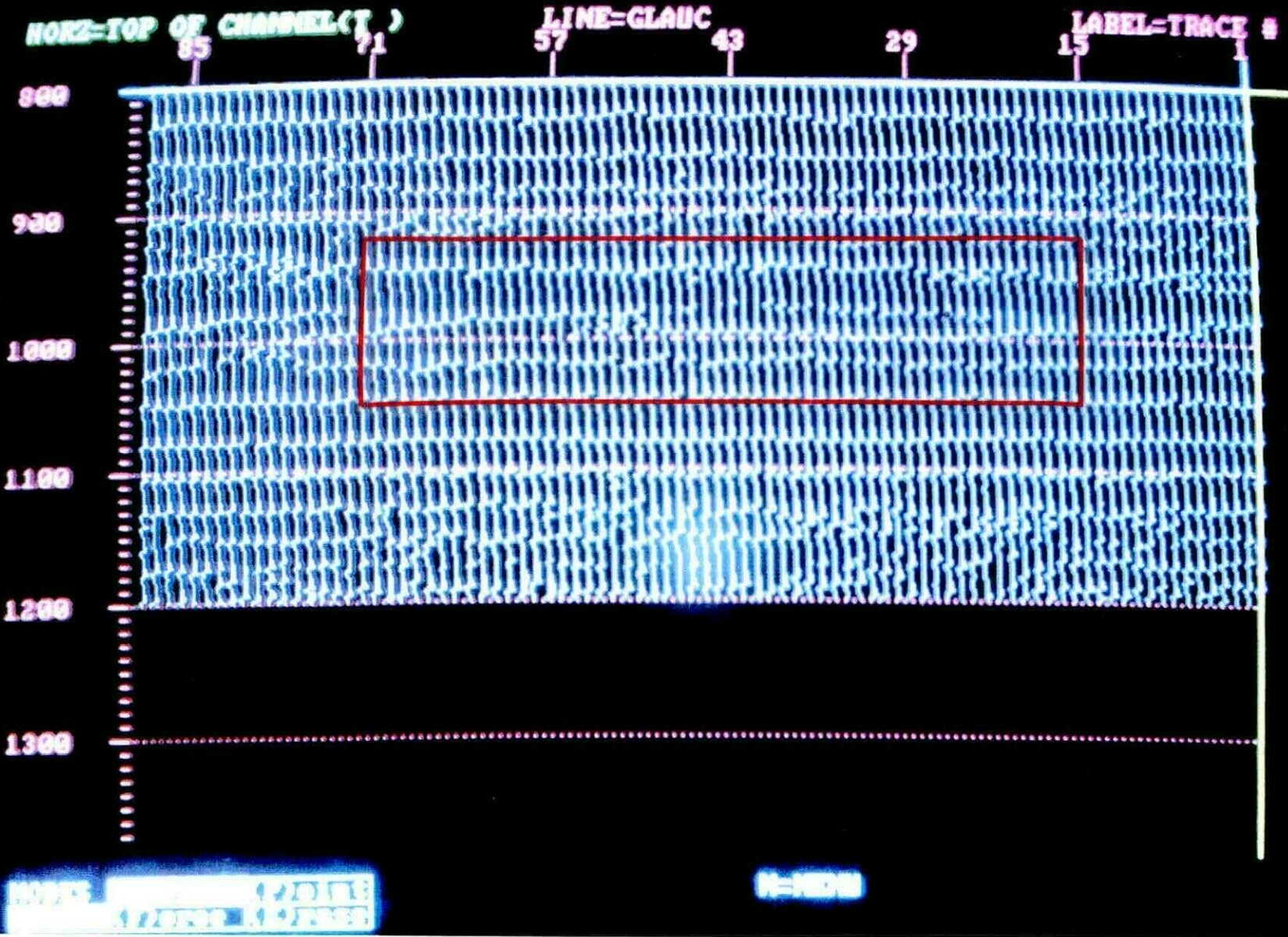


Figure 20. The instantaneous phase plot for the near-offset stack.

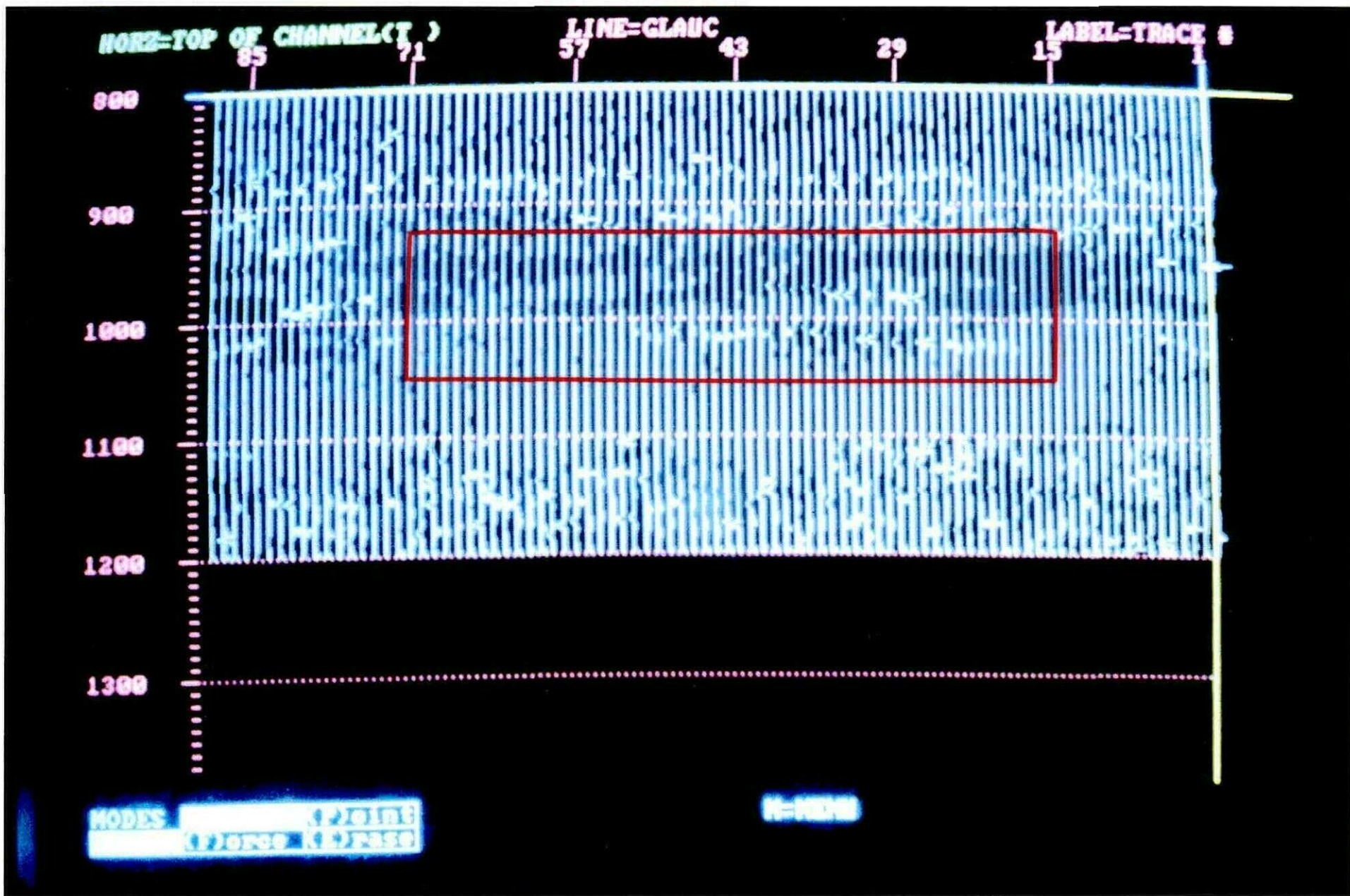


Figure 22. The instantaneous frequency plot for the full-offset stack.

328

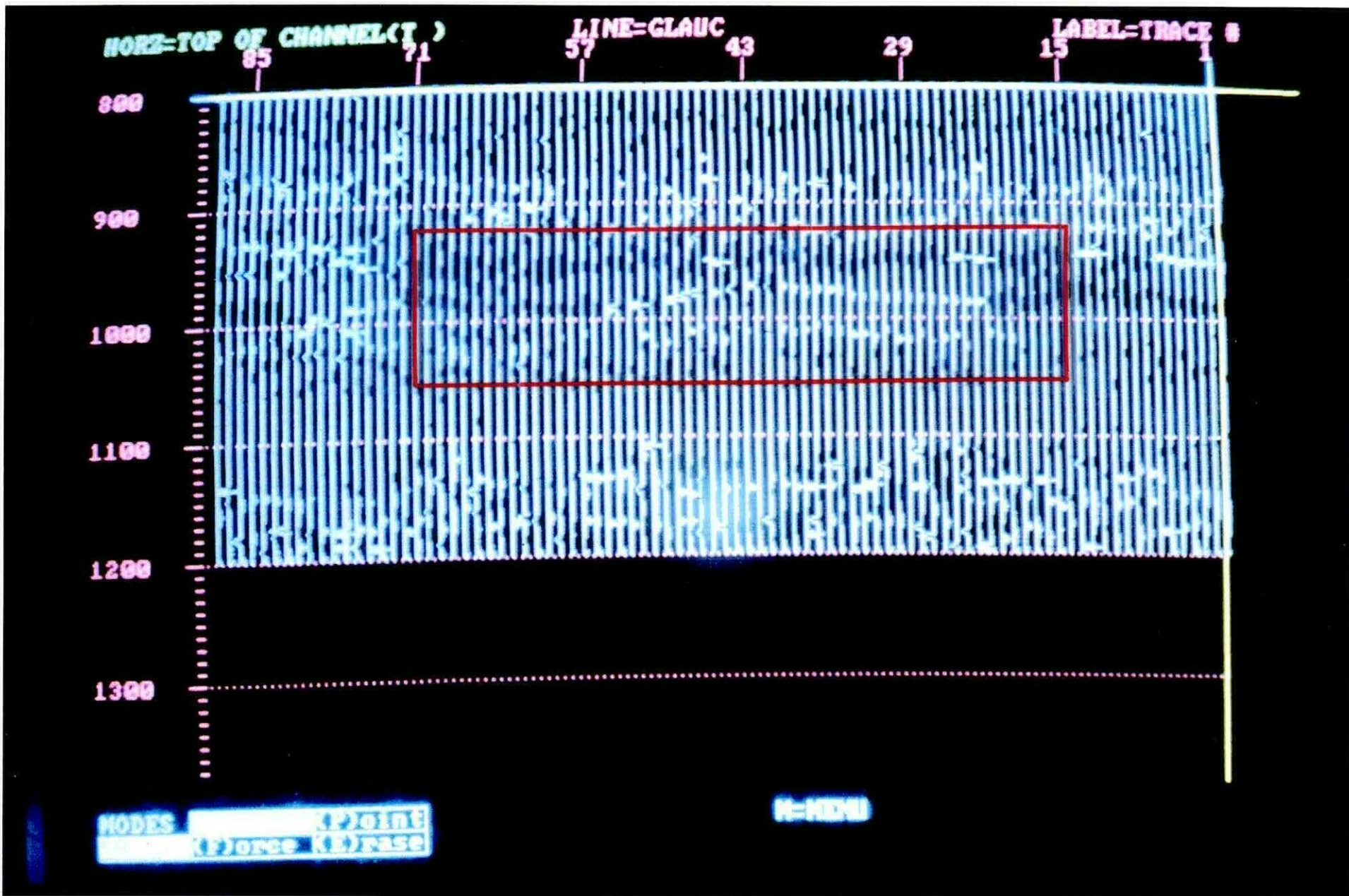


Figure 23. The instantaneous frequency plot for the near-offset stack.

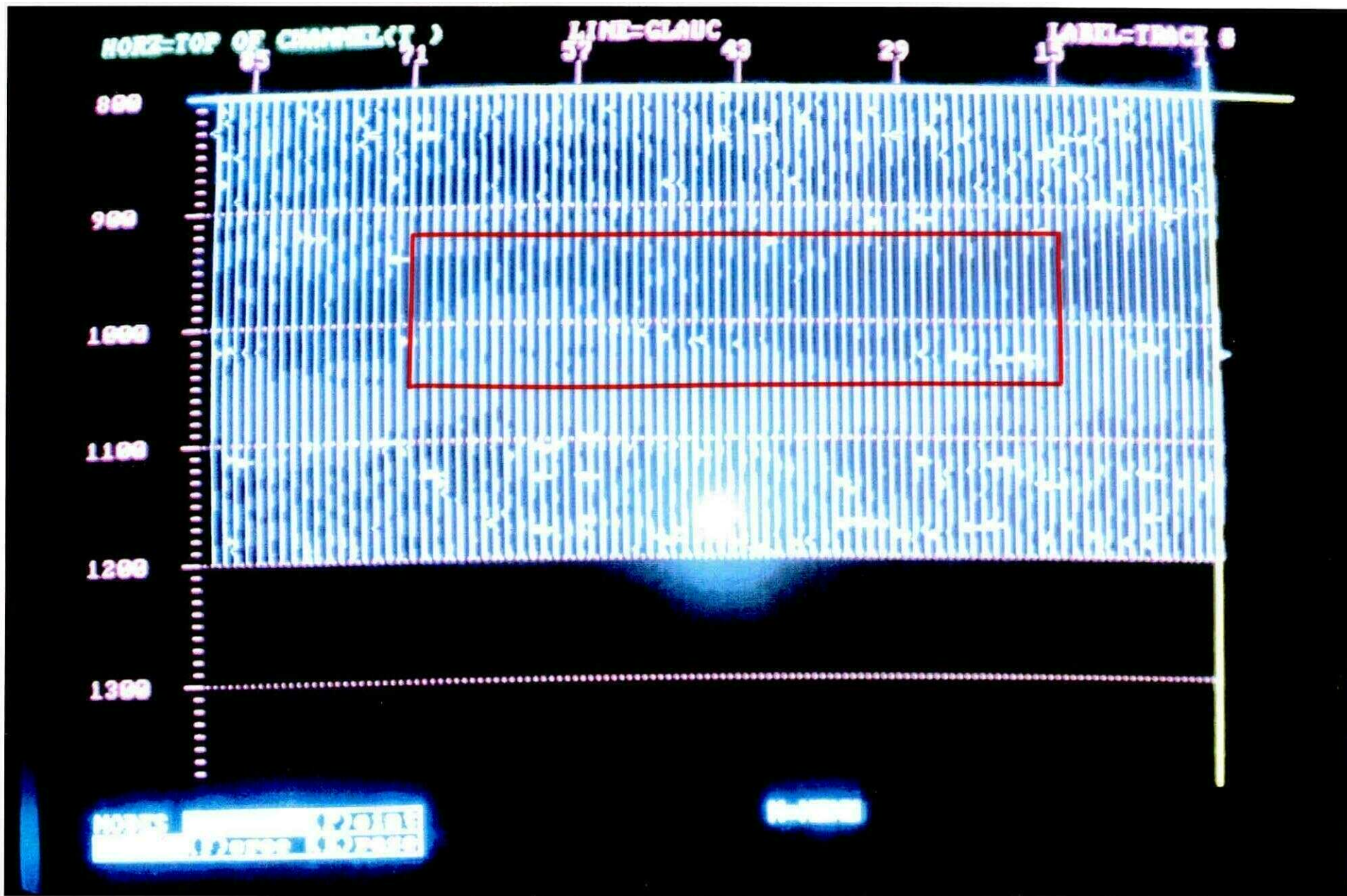


Figure 24. The instantaneous frequency plot for the mid-offset stack.